

POLITECNICO DI TORINO

Master's Degree in Civil Engineering



**Master thesis:**

**FLUTTER ANALYSIS OF SUSPENSION  
BRIDGES IN ANSYS: THE AKASHI KAIKYO  
BRIDGE CASE-STUDY**

Supervisors: Prof. Alberto Carpinteri

Dr. Gianfranco Piana

Candidate:

Francesco Di Agabito

Academic Year 2017/2018

# Ringraziamenti

Porgo i miei più sentiti ringraziamenti all'istituzione Politecnico di Torino ed ai docenti che mi hanno accompagnato durante il corso di studi ed hanno contribuito alla mia crescita personale e delle mie conoscenze.

Un particolare ringraziamento va al Prof. Alberto Carpinteri che ha fatto crescere in me la curiosità riguardo specifiche criticità dell'ingegneria strutturale, come quelle riguardanti i ponti sospesi e che ha gentilmente accettato l'importante incarico di essere il mio relatore durante il percorso di studi, finalizzato alla realizzazione della mia tesi di laurea. Un sentito ringraziamento al Dott. Gianfranco Piana, che mi ha seguito con grande professionalità e disponibilità nel tortuoso e ricco di insidie percorso che la redazione di una tesi di laurea nasconde.

Si ringrazia l'Ing. Gaetano Miraglia per i preziosi suggerimenti forniti nell'utilizzo del programma ANSYS, durante le prime fasi del presente lavoro.

Gran parte del merito per il raggiungimento di questo mio traguardo va a tutta la mia famiglia ed in particolare ai miei genitori, Antonio e Rina, che mi hanno applaudito ed hanno gioito con me nei traguardi raggiunti e che soprattutto hanno avuto la pazienza e l'attenzione di essermi vicini ed incoraggiarmi nei momenti difficili, che un percorso di laurea impegnativo come questo presenta, non perdendo mai la fiducia in me.

# Abstract

The aim of the present thesis is to analyse the behaviour of suspension bridges under wind by a commercial finite element software; in particular, the longest suspension bridge in the world – the *Akashi Kaikyo Bridge* – was selected as a case study. The research is focused on the most dangerous phenomenon that may occur in this kind of structures, i.e., flutter instability. The goal is to explore different numerical models in order to compare the results to those obtained by different approaches, both analytical and numerical.

The first part begins with theoretical considerations regarding the description of wind effects on suspension bridges. Analytical and numerical approaches, developed by various authors, are presented. A study from the literature, performed on an ideal suspension bridge, is considered at first. Afterwards, different analyses performed, by several authors, on the *Akashi Kaikyo Bridge* to evaluate its natural frequencies and critical flutter wind speed are presented. The results are taken as reference values in order to make a comparison with the numerical results obtained in this thesis using *ANSYS* software, presented in the following part.

The second part begins with a “validation problem”: a modal analysis of a simple 2D structure was performed in *ANSYS* before studying the *Akashi Kaikyo Bridge*. Then, different models and analysis of the *Akashi Kaikyo Bridge* performed in this thesis are presented. A “Fish-bone” model was firstly implemented. A preliminary modal analysis was run to evaluate the natural frequencies and mode shapes of the structure. Afterwards, a flutter analysis was run by considering all three unsteady aerodynamics loads acting on the deck, i.e. Lift, Drag and Moment, modelled by the so-called *flutter derivatives*. In this way, it was possible to evaluate the critical flutter speed and frequency, as well as to identify the critical mode shape. The numerical model of the bridge was then improved by modelling the deck as a 3D truss beam, as in the real case. As for the previous model, a modal analysis was performed before studying flutter instability. Three different approaches were followed to evaluate the flutter speed and frequency, and the corresponding mode shape: (i) Lift, Drag and Moment all modelled as unsteady actions; (ii) Lift and Moment treated as unsteady actions, Drag force modelled as steady load; (iii) Lift and Moment modelled as unsteady actions, Drag force totally neglected.

In conclusion, the results obtained by the three different analyses are compared to literature data about the *Akashi Kaikyo Bridge*, as well as to results obtained by other methods described in the first part of the thesis.

# Table of contents

RINGRAZIAMENTI .....	I
ABSTRACT .....	II
TABLE OF CONTENTS .....	IV
LIST OF FIGURES .....	VI
LIST OF TABLES .....	IX
PART 1 .....	11
CHAPTER 1 INTRODUCTION .....	12
1.1 HISTORICAL DEVELOPMENT.....	13
CHAPTER 2 WIND LOAD .....	15
2.1 INTRODUCTION TO FLUTTER OF LONG-SPAN BRIDGES .....	16
2.1.1 <i>Steady aerodynamic analysis</i> .....	19
Static divergence.....	21
2.1.2 <i>Two-degree of freedom flutter</i> .....	23
2.1.3 <i>One-degree of freedom flutter</i> .....	25
CHAPTER 3 NUMERICAL FULL-BRIDGE MODELLING AND DESCRIPTION OF THE CASES STUDY.....	28
3.1 A SALVATORI AND BORRI STUDY .....	29
3.1.1 <i>Analysis method</i> .....	29
3.1.2 <i>Analysis results</i> .....	34
3.2 AKASHI KAIKYO BRIDGE .....	35
3.2.1 <i>Miyata and Katsuchi studies</i> .....	37
Flutter analysis .....	38
3.2.2 <i>D'Argenio study</i> .....	40

3.2.3 Maldera study: series of functions.....	44
PART 2.....	50
CHAPTER 4 TEST PROBLEMS IN ANSYS.....	51
4.1 DYNAMICS OF STRAIGHT PRESTRESSED CABLE.....	52
4.1.1 Numerical example.....	53
4.2 HEAVY CABLE SMALL OSCILLATIONS.....	55
4.2.1 Numerical example.....	56
4.3 REAL CASE NUMERICAL EXAMPLE: SINGAPORE SUSPENSION FOOTBRIDGE.....	58
4.4 SALVATORI-BORRI IDEAL BRIDGE.....	61
CHAPTER 5 AKASHI KAIKYO BRIDGE ANALYSIS.....	64
5.1 “FISH-BONE” MODEL.....	65
5.1.1 Flutter analysis.....	68
Analysis results.....	73
5.2 “TRUSS-BEAM” DECK MODEL.....	75
5.2.1 Modal analysis.....	76
5.2.2 Flutter analysis.....	77
Lift, Drag and Moment unsteady analysis.....	78
L-M unsteady, Drag steady actions.....	80
Lift and Moment unsteady actions.....	82
CHAPTER 6 CONCLUSIONS.....	83
REFERENCES.....	86

## List of figures

Figure 1-1: Suspension Bridge Thangtong Gyalpo [1]	13
Figure 1-2: Suspension bridge at Jacob's Creek in Westmoreland County[2]	14
Figure 2-1: Tacoma Narrows Bridge falls[3]	15
Figure 2-2: Golden Gate Bridge	16
Figure 2-3: Representation of static and dynamic instability[4]	18
Figure 2-4: Representation of the forces acting on the deck	19
Figure 2-5: $CD, CL, CM$ graphs for different bridge sections and different angles of attach	20
Figure 2-6: Simplified model with single degree of freedom (left), variation of $CM$ with angle of attack $\alpha$ (right)	21
Figure 2-7: Graphics representation of critical wind speed	22
Figure 2-8: Two degrees of freedom simplify model	23
Figure 2-9: Examples of flutter derivates	24
Figure 2-10: Definition flutter critic speed	25
Figure 3-1: Forces acting on bridge section[5]	29
Figure 3-2: Representation of discrete structural model	30
Figure 3-3: Flow chart of stability analysis in frequency domain	32
Figure 3-4: Geometry of the bridge	33
Figure 3-5: Time history fluctuations	34
Figure 3-6: Critical mode-shape (absolute value on the left, phase angle on the right)	35
Figure 3-7: Akashi Kaikyo Bridge section	36
Figure 3-8: Akashi Kaikyo Bridge profile	36
Figure 3-9: Scale model used by Miyata	37
Figure 3-10: Fish bone model used in ADISNOL3D	37
Figure 3-11: Real parts(left) and imaginary part (right) behaviour for 2 mode analysis[6]	39
Figure 3-12: Real parts(left) and imaginary part (right) behaviour for 17 mode analysis[6]	39
Figure 3-13: Flexural and torsional frequencies behaviour respect wind speed, of Akashi Kaikyo Bridge, obtained with MATLAB	41

Figure 3-14: Solutions for individuation of critic flutter speed with second-order effects: anti-symmetric mode (left), symmetric mode (right)	43
Figure 3-15: Solutions for individuation of critic flutter speed without second-order effects: anti-symmetric mode (left), symmetric mode (right)[7]	43
Figure 3-16: Main span of suspension bridge subjected to steady actions $px, mz$	45
Figure 3-17: Flexural and torsional, real and imaginary part behaviour respect wind speed, of Akashi Kaikyo Bridge, obtained with MATLAB, one approximating function[8]	47
Figure 3-18: Behaviour of torsional and flexural frequencies respect wind speed, obtained with one and four approximating functions[8]	48
Figure 4-1: Straight cable subjected to pretension T	52
Figure 4-2: Representation of BEAM188 element[9]	53
Figure 4-3: Mode 1, 2.3595 Hz; Figure 4-4: Mode 2, 4.7209 Hz	54
Figure 4-5: Mode 3, 7.0865 Hz; Figure 4-6: Mode 4, 9.4581 Hz	54
Figure 4-7: Mode 5, 11.838 Hz	54
Figure 4-8: Heavy cable fluctuations	55
Figure 4-9: Mode 1 anti-symmetric, 0.09464 Hz; Figure 4-10: Mode 1 symmetric, 0.1323 Hz	57
Figure 4-11: Mode 2 anti-symmetric, 0.1937 Hz; Figure 4-12: Mode 2 symmetric, 0.1793 Hz	57
Figure 4-13: Mode 3 anti-symmetric, 0.2918 Hz; Figure 4-14: Mode 3 symmetric, 0.2459 Hz	57
Figure 4-15: Geometrical properties of Singapore Suspension Footbridge	59
Figure 4-16: LINK180 representation[11]	59
Figure 4-17: Mode 1 symmetric, 1.4531 Hz; Figure 4-18: Mode 1 anti-symmetric, 2.0935 Hz	60
Figure 4-19: Mode 2 symmetric, 4.6431 Hz	60
Figure 4-20: “Fish-bone” ANSYS numerical model	61
Figure 4-21: Mode 1 H-S, 0.08456 Hz; Figure 4-22: Mode 1 V-A, 0.1052 Hz	62
Figure 4-23: Mode 1 V-S, 0.1426 Hz; Figure 4-24: Mode 1 H-A, 0.1762 Hz	62
Figure 4-25: Mode 1 T-S, 0.3432 Hz; Figure 4-26: Mode 1 T-A, 0.3457 Hz	63
Figure 5-1: Dry air injection system	65
Figure 5-2: View of Akashi Kaikyo Bridge	65
Figure 5-3: Akashi Kaikyo “Fish-bone” numerical model	66
Figure 5-4: Mode 1 H-S, 0.0366 Hz; Figure 5-5: Mode 1 V-S, 0.0593 Hz	66
Figure 5-6: Mode 1 H-A, 0.0654 Hz; Figure 5-7: Mode 1 V-A, 0.0815 Hz	67
Figure 5-8: Mode 1 T-S, 0.132 Hz; Figure 5-9: Mode 1 T-A, 0.203 Hz	67
Figure 5-10: Deck section representation	69

Figure 5-11: Matrix27 ANSYS element[14]	70
Figure 5-12: Hybrid finite element model for flutter analysis in ANSYS	71
Figure 5-13: Hybrid ANSYS model of Akashi Kaikyo Bridge, with MATRIX27 elements	72
Figure 5-14: Flutter derivatives for Akashi Kaikyo Bridge	73
Figure 5-15: Real part eigenvalue (left), imaginary part (right)	74
Figure 5-16: “Truss-beam” deck ANSYS numerical model	75
Figure 5-17: Akashi Kaikyo Bridge rendering model	76
Figure 5-18: Deck section and actions representation	78
Figure 5-19: Real (left) and imaginary (right) part of the solution	78
Figure 5-20: Critical flutter mode-shape	79
Figure 5-21: Real (left) and imaginary (right) part of the solution	81
Figure 5-22: Real (left) and imaginary (right) part of the solution	82

## List of tables

Table 3-1: Geometrical properties Salvatori-Borri bridge	33
Table 3-2: Geometrical and mechanical properties of the Akashi Kaikyo Bridge	37
Table 3-3: Comparison of natural frequencies[6]	38
Table 3-4: Comparison of different flutter analysis[6]	40
Table 3-5: Aero-dynamic properties of Akashi Kaikyo Bridge	40
Table 3-6: Natural frequencies of Akashi Kaikyo Bridge obtained with MATLAB program[7]	42
Table 3-7: Critic flutter wind speed and frequencies for symmetric and anti-symmetric configurations, with second-order effects[7]	43
Table 3-8: Critic flutter wind speed and frequencies for symmetric and anti-symmetric configurations, without second-order effects	43
Table 3-9: Natural frequencies of Akashi Kaikyo Bridge obtained with four-function analysis	47
Table 3-10: Flutter critic speeds with second-order effects, using four approximating functions[8]	48
Table 3-11: Flutter critic speeds without second-order effects, using four approximating functions[8]	48
Table 3-12: Results with second-order and standard analysis, with four and one approximating functions	49
Table 4-1: Straight cable properties	53
Table 4-2: Results comparison and relative errors[10]	55
Table 4-3: Geometrical properties of heavy cable	56
Table 4-4: Results comparison and relative errors	58
Table 4-5: Mechanical and geometrical properties of Singapore Suspension Footbridge	59
Table 4-6: Results with different methods and relative errors	61
Table 4-7: Natural frequencies of Salvatori-Borri bridge	63
Table 5-1: Akashi Kaikyo Bridge modal analysis results	68
Table 5-2: Akashi Kaikyo Bridge flutter analysis results comparison	74
Table 5-3: Geometrical properties of “truss-beam” deck	76
Table 5-4: Modal analysis “truss-beam” model results	77

Table 5-5: Akashi Kaikyo Bridge flutter analysis, with three n-s actions, results comparison	79
Table 5-6: Akashi Kaikyo Bridge flutter analysis, with two n-s actions and Drag steady, results comparison	81
Table 6-1: “Fish-bone” model flutter analysis results comparison	84
Table 6-2: “Truss-beam” model flutter critic speeds and frequencies comparison	85

# **PART 1**

# CHAPTER 1

## INTRODUCTION

In a suspension bridge, the traffic-carrying deck is supported by a series of wire ropes that hang from massive cables draped between tall towers. The *Brooklyn Bridge* in New York City and the *Golden Gate Bridge* in San Francisco are two of the most famous suspension bridges. The *Akashi Kaikyo Bridge* in Japan, which was completed in 1998, is characterised by the world's longest suspension span, precisely of 1991 m.

It is possible to divide the suspension bridges evolution in three generations.

- The first generation consist of a lot of framework deck bridges, built in the USA between the end of 19<sup>th</sup> and the beginning of 20<sup>th</sup> century (*Brooklyn* 1883, *Golden Gate* 1937). The span of this kind of bridges reach a maximum length of 1000 m. The framework deck gives a great flexural and torsional stiffness to the structure, but the big wind resistance is obtained with important weights of all the elements, with large structural deformation under variable loads. The *Akashi Kaikyo Bridge* (built in 1998), with his 1991 m of span, represents the maximum limit for this bridges' generation.
- The second generation includes aerodynamic deck bridges, with single caisson. Built in the second half of 20<sup>th</sup> century in Europe (*Humber Bridge* 1981, *Bosforo* 1973), these bridges have a span, whose length varies between 1000 m and 1600 m. The aerodynamic caisson presents small deformations under wind actions and it has smaller weight. This kind of deck maintains an important torsional stiffness, but for big spans, it is necessary to increase the deck height that causes the growth of wind resistance and the structural weight. For this generation, it is possible to define a maximum span limit about 2000 m, where the stability contribution given by the deck is negligible.

- The third generation was born with the design of *Messina Bridge*, characterised by a deck structure that allows an increase of maximum span length. The deck section is composed by multiple caissons with aerodynamic shapes, it offers a very small wind resistance and it is stable respect to the aero-elastic instability phenomena. The structural stability depends on suspension system, which gives enough stiffness at the central span of 3300 m.

## 1.1 Historical development

One of the oldest of engineering forms, suspension bridges were constructed by primitive peoples using vines for cables and mounting the roadway directly on the cables. A much stronger type was introduced in India about the 4th century ad that used cables of plaited bamboo and later of iron chain, with the roadway suspended. In modern times, the suspension bridge provided an economical solution to the problem of long spans over navigable streams or where there are sites which present difficulties in placing piers in the stream. British, French, American, and other engineers of the late 18th and early 19th centuries encountered serious problems of stability and strength against wind forces and heavy loads; failures resulted from storms, heavy snows, and droves of cattle.

Earliest versions of suspension bridges were built by Thangtong Gyalpo, Tibetan saint and bridge-builder (among other things) from the 15th century. He built over 58 iron chain suspension bridges around Tibet and Bhutan and one of his bridges survived until 2004 when it was destroyed by a flood. Most of his bridges had chains as suspension cables while his early bridges used ropes from twisted willows or yak skins, as illustrated in *Figure 1-1*.



*Figure 1-1: Suspension Bridge Thangtong Gyalpo [1]*

The first iron chain suspension bridge on the soil of United States was the made at *Jacob's Creek* in *Westmoreland County*, Pennsylvania in 1801. This bridge, as illustrated in *Figure 1-2* was the first to have all the necessary components of a modern suspension bridge and was designed by James Finley who patented a system for suspending a rigid deck from a bridge's cables in 1808. That years can be considered as the beginning of the era of the modern suspension bridges. After that, two bridges were built in England: *Dryburgh Abbey Bridge* (built in 1817) and *Union Bridge* (built in 1820). The first large bridge that used the technique invented by Finley was the bridge over the *Menai Straits* in Wales built by Thomas Telford and completed in 1826. Cables consisting of many strands of wire for suspension were used instead of chains for the first time in 1930 by French engineers. Soon John Roebling, American inventor, found a way to spin the cables in loco instead of transporting them prefabricated. He also invented rigid deck platform which is stiffened with trusses.

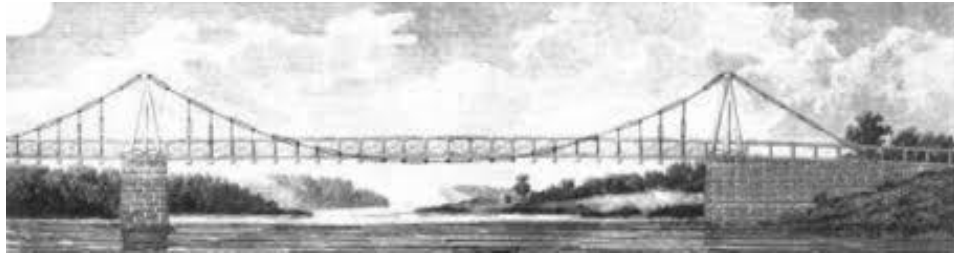


*Figure 1-2: Suspension bridge at Jacob's Creek in Westmoreland County[2]*

Since then suspension bridges became popular because they allowed to overcome spaces that otherwise could not be overcome with conventional methods. The main advantage is that it can be made with longer spans respect to all other types of bridges; it is cheaper bridge type (even with longer spans) because it uses less material; during construction it does not require access from below so it doesn't matter what is present below nor how high is bridge. Furthermore, it is more earthquake-proof than other types; and it can be modified easily to accommodate wider vehicles or to add additional lanes. However, on the other hand, it also has its disadvantages: it must be made very stiff or aerodynamic, so high winds wouldn't cause vibrations; and it is very difficult for to carry heavy rail traffic compared to other bridge types because of relatively lower stiffness of a board. When compared, suspension bridges are often compared by the length of their main span (longest span they have). *Akashi Kaikyo Bridge* is the suspension bridge with the longest span in the world since 1998. Its 1991 meters connects Kobe and Awaji Island in Japan. At the second place in this type of list is present the *Xihoumen Bridge* with 1650 meters on the Zhoushan Archipelago, the largest offshore island group in China.

## CHAPTER 2

# WIND LOAD

The beginning of the history of big suspension bridge dates back to 1826, when the construction of the *Bridge Menai* ended. Designed by the English engineer Telford, it was very important because it connected Anglesey land and England with a main span of 176 m. Unfortunately, the bridge had a short life, in fact it was destroyed by a wind storm after some months.

In Europe and USA, in 19<sup>th</sup> century, several bridges fell down, under wind action because no analysis regarding this load was done before the bridges construction.

When, in West Virginia (USA), the *Wheeling Bridge* fell, the analysis of wind effects starts for the design of big span bridges. Thanks to the improvement of the design methods, the bridges were realized with an increasing slenderness and the ratio between the height of deck and main span length became smaller.

Another important example of suspension bridge is the *Golden Gate* in San Francisco, that in few times presented fluctuations under wind action of 3 m in horizontal plane.



Figure 2-1: Tacoma Narrows Bridge falls[3]

A structure with a more important slenderness was the *Tacoma Narrows Bridge* (*Figure 2-1*), with a main span of 853 m, built in 1940 in west coast of USA by Moisseif. This bridge was characterized by an insufficient stiffness to counteract wind dynamic actions. The structure, closed at the end of construction, started to propose vertical fluctuations and, during a storm with a wind speed of 50 km/h, had torsional vibrations with increasing magnitude and fell in some hours. After this disaster, the researchers and technicians decided to focus especially on the studies of the bridge aerodynamics and the analyses on aircraft wings were used for big span bridges to evaluate the actions of wind on the decks. The most dangerous phenomenon in suspension bridge is flutter, caused by resonance between unsteady forces produced by moving structure and its fluctuation.



*Figure 2-2: Golden Gate Bridge*

## **2.1 Introduction to flutter of long-span bridges**

The aeroelastic instability has a great importance in big span suspension bridges. Aero-elastic instability by flutter on the deck is caused by matching of two modes of fluctuation, flexural and torsional, with similar deformed shapes. Relative frequencies are approached by wind action, that gives energy to the system. The matching of 2 degrees of freedom is the characteristic aspect of this phenomenon: vertical and torsional motion are timed on the same frequency, equivalent to the average value between the two fluctuations.

Wind effects on decks are correctly evaluated with time domain analysis, using non-linear numerical simulation, with the definition of appropriate wind stories and experimental test in wind tunnel. In this case, to understand the real behaviour of the main structure, scaled models are used to perform all the analyses. Furthermore, also sections of the deck are studied, to focus on the behaviour of the bridge and the local effects.

But theoretical models are very important because they allow to evaluate at least the order of magnitude of wind speed through which the instability may occur.

The analysis in frequencies domain is possible if a linearization of phenomenon is realised, with the introduction of strength coefficients obtained by scaled models.

The reasons why it is possible to consider analytic approach are:

- Structure has an elastic-linear behaviour, with a sinusoidal exponentially dumped response;
- The transition between stable and instable configuration happens in conditions of oscillatory motion about equilibrium configuration on average wind condition.

These hypotheses allow to perform flutter analysis for a linear elastic system. The dynamic problem could be represented, in linearized form, with this equation:

$$[M] \cdot \ddot{\delta}(T) + [K] \cdot \delta(T) = 0 \quad (2-1)$$

where:

- $\delta$ : is the displacements vector, time depending;
- $[M]$ : is the mass matrix;
- $[K]$ : is the tangent stiffness matrix.

The necessity of performing stability linear analyses, lead the researchers to consider harmonic time disturbances, because dynamic evolution of the structure could be divided in a series of harmonic contributions with a Fourier process. It is assigned an harmonic disturbance  $(\delta) = (\delta_0) \cdot e^{i\omega t}$ , where  $\delta_0$  is the initial displacement, and initial conditions. The system of differential equation (2.1) has trivial modes as solution, except for modes with  $\omega$  pulsation, that satisfy characteristic equation:

$$([K] - \omega^2[M])\{\delta\} = (0) \quad (2-2)$$

The solution of the system allows to obtain eigenvalues  $\omega$  and eigenvectors  $\{\delta\}$  in undeformed configuration of the structure. The equation represents stress-free configuration of suspension bridge, where it is possible to find the mass matrix and the structural stiffness of the system. Correct modal analyses for these kinds of structures could be performed using static prestressed configuration, assuming this form:

$$([K] + [K]_g - \omega^2[M])\{\delta\} = (0) \quad (2-3)$$

So, defining:

$$[\bar{K}] = ([K] + \lambda[K]_g) \quad (2-4)$$

it is possible to obtain eigenvalue  $\omega_j$  ( $j=1,2,\dots$  d.o.f.) as a function of load factor  $\lambda$ . The equilibrium can become unstable in correspondence of the critical value  $\lambda_c$ .

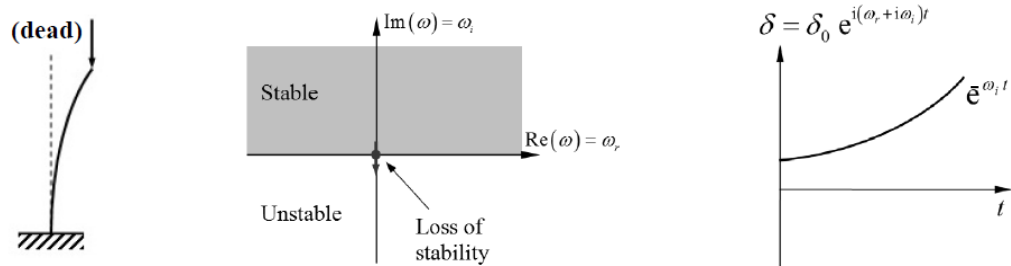
Considering the  $j^{th}$  eigenvector:

$$\{\delta_j\} = \{\delta_{0j}\} \cdot e^{i\omega_j t} = \{\delta_{0j}\} \cdot e^{i(\omega_r + i\omega_i)t} = \{\delta_{0j}\} \cdot e^{i\omega_r t} \cdot e^{-\omega_i t} \quad (2-5)$$

It is possible to consider that the stability depends on the sign of the imaginary part of the eigenvalue  $\omega_j$ :

- If  $\omega_{ij} > 0$  for each eigenvalue, equilibrium is stable;
- If  $\omega_{ij} = 0$  at least for one eigenvalue, equilibrium is metastable;
- If  $\omega_{ij} < 0$  at least for one eigenvalue, equilibrium is unstable.

### Static instability



### Dynamic instability (flutter)

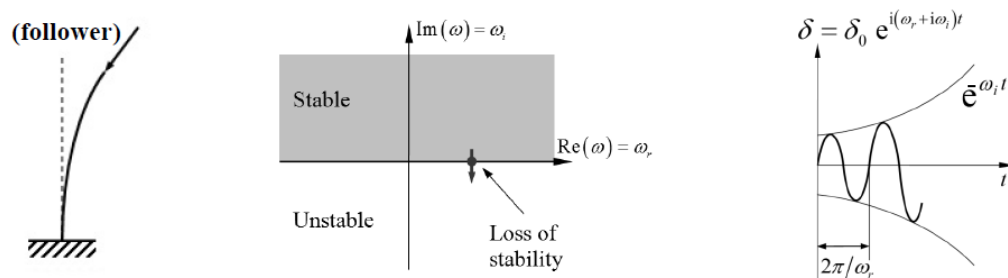


Figure 2-3: Representation of static and dynamic instability[4]

For conservative models, the pulsations (angular frequencies) can be real for stable system or imaginaries for unstable ones. Equilibrium becomes unstable if the smallest characteristic pulsation assumes zero value, or if the stiffness matrix shows a singularity. When the equilibrium is unstable, the structure, after a perturbation, leaves its configuration and it may assume another stable configuration. This instability is called divergence or static

bifurcation of equilibrium and its characterization can be evaluated even without a dynamic approach.

In non-conservative systems, equilibrium becomes instable when the smallest characteristic pulsation assumes zero value, as in conservative system, or when two pulsations tend one to each other and they become complex conjugates, or again when a single pulsation becomes complex. In this case, an alternative equilibrium configuration for the structure, doesn't exist. The case of two pulsations complex conjugates display a flutter instability phenomenon and the load condition that generate the coincidence between two pulsations is called flutter load.

To perform a complete analysis of the bridge, it is possible to consider three different approaches:

- Steady aerodynamic analysis;
- 1 degree of freedom flutter analysis;
- 2 degrees of freedom flutter analysis.

### 2.1.1 Steady aerodynamic analysis

The analysis is performed considering a static condition of the bridge and, with the application of plane forces in x and y directions and torque moment; stability is evaluated with respect to the deformed shape of the deck under wind action and its instability. It is possible to consider laminar flow on deck direction that generates steady forces.

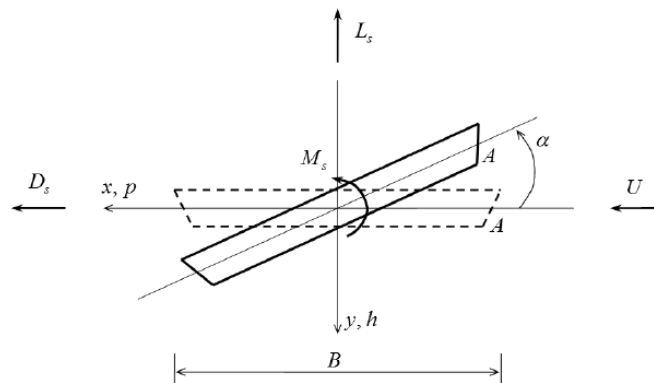


Figure 2-4: Representation of the forces acting on the deck

Drag force in x direction, lift force in y direction and moment around z axis are shown in the following equations:

$$D_s = \frac{1}{2} \cdot \rho \cdot U^2 \cdot B \cdot C_D(\alpha) \quad (2-6)$$

$$L_s = \frac{1}{2} \cdot \rho \cdot U^2 \cdot B \cdot C_L(\alpha) \quad (2-7)$$

$$M_s = \frac{1}{2} \cdot \rho \cdot U^2 \cdot B^2 \cdot C_M(\alpha) \quad (2-8)$$

where:

- $\rho$ : air density [kg/m<sup>3</sup>];
- $U$ : average wind speed [m/s];
- $B$ : deck width [m];
- $C_D, C_L, C_M$ : non-dimensional static aerodynamic factors of drag, lift and moment;
- $\alpha$ : angle of attach [deg].

Aerodynamic factors are evaluated in wind tunnel with a scale section, where it is possible the variation of  $\alpha$ , so forces are obtained. Dividing  $D_s, L_s, M_s$  by  $\frac{1}{2} \cdot \rho \cdot U^2 \cdot B$  are evaluated  $C_D, C_L, C_M$ .

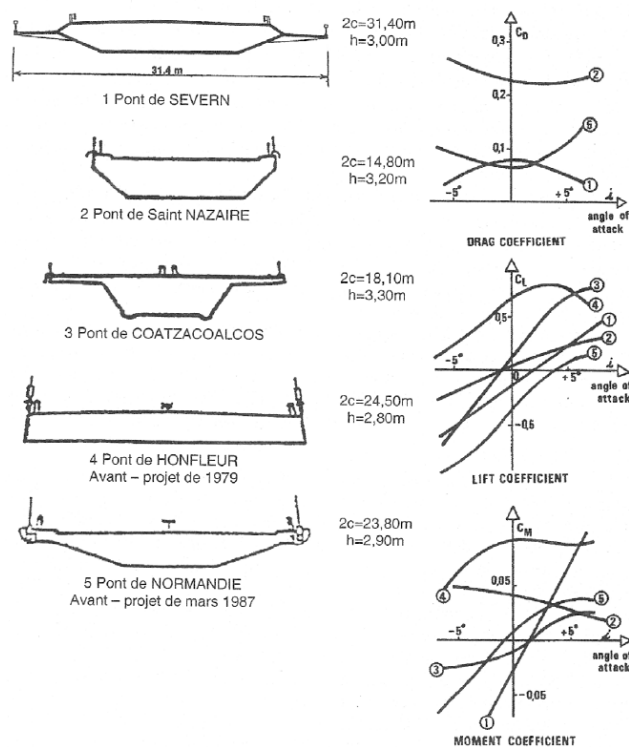


Figure 2-5:  $C_D, C_L, C_M$  graphs for different bridge sections and different angles of attach

For small angles of attack the  $C_D, C_L, C_M$  can be linearized and then Eq. 2-6, 2-7, 2-8 become:

$$D_s = \frac{1}{2} \cdot \rho \cdot U^2 \cdot B \cdot C_D(0) \quad (2-9)$$

$$L_s = \frac{1}{2} \cdot \rho \cdot U^2 \cdot B \cdot \left( C_L(0) + \left( \frac{dC_L}{d\alpha} \right) \cdot \alpha \right) \quad (2-10)$$

$$M_s = \frac{1}{2} \cdot \rho \cdot U^2 \cdot B^2 \cdot \left( C_M(0) + \left( \frac{dC_M}{d\alpha} \right) \cdot \alpha \right) \quad (2-11)$$

### Static divergence

Static divergence is an instability phenomenon where the in-wind natural frequency of a mode decreases to zero as the wind velocity increases. This is a static instability in torsion that occurs because of the loss of torsional stiffness.

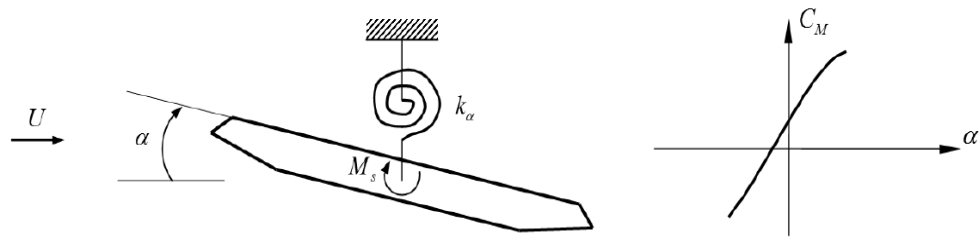


Figure 2-6: Simplified model with single degree of freedom (left), variation of  $C_M$  with angle of attack  $\alpha$  (right)

It is possible to define:

- Resisting elastic moment:

$$M_e = k_a \cdot \alpha \quad (2-12)$$

$k_a$ : torsional stiffness [Nm/m]

- Acting aerodynamic moment:

$$M_s = \frac{1}{2} \cdot \rho \cdot U^2 \cdot B^2 \cdot \left( C_M(0) + \left( \frac{dC_M}{d\alpha} \right) \cdot \alpha \right) \quad (2-13)$$

It is possible to observe that the instability of  $M_s$  effect increases with wind speed.

For the equilibrium it is necessary to have  $M_e = M_s$ , and thus:

$$k_\alpha \cdot \alpha = \frac{1}{2} \cdot \rho \cdot U^2 \cdot B^2 \cdot \left( C_M(0) + \left( \frac{dC_M}{d\alpha} \right) \cdot \alpha \right) \quad (2-14)$$

It is possible put on first member terms depending by  $\alpha$ :

$$\left[ k_\alpha - \frac{1}{2} \cdot \rho \cdot U^2 \cdot B^2 \cdot \left( \frac{dC_M}{d\alpha} \right) \right] \cdot \alpha = \frac{1}{2} \cdot \rho \cdot U^2 \cdot B^2 \cdot C_M(0) \quad (2-15)$$

where total stiffness of system is expressed by:

$$k_{tot} = \left[ k_\alpha - \frac{1}{2} \cdot \rho \cdot U^2 \cdot B^2 \cdot \left( \frac{dC_M}{d\alpha} \right) \right] \quad (2-16)$$

By the condition  $k_{tot} = 0$ , it is possible to evaluate critical speed of torsional divergence:

$$U_D = \sqrt{\frac{2 \cdot k_\alpha}{\rho \cdot B^2 \cdot \left( \frac{dC_M}{d\alpha} \right)}} \quad (2-17)$$

An important aspect is the presence of deck width B as denominator of the expression, in fact, if B increase there is the reduction of critical speed.

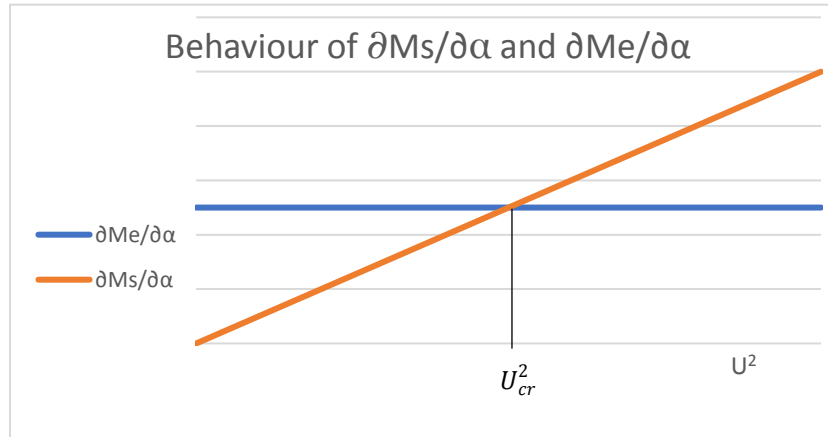


Figure 2-7: Graphics representation of critical wind speed

Considering a graphic behaviour of the derivates of  $M_s$  and  $M_e$  with respect to the angle of inclination  $\alpha$ , it is clear how the derivate of  $M_s$  with respect to the angle of inclination  $\alpha$  has a linear trend respect to the wind speed powered to two ( $U^2$ ), while the derivate of  $M_e$  assumes a constant value.

There are two possibilities:

- When  $\frac{\partial M_e}{\partial \alpha} > \frac{\partial M_s}{\partial \alpha}$  the system is stable;
- When  $\frac{\partial M_e}{\partial \alpha} < \frac{\partial M_s}{\partial \alpha}$  the system is instable.

The graph shows that when there is the intersection between two lines of stabilising and destabilising moments,  $\frac{\partial M_s}{\partial \alpha}$  become greater than  $\frac{\partial M_e}{\partial \alpha}$  and in this point the wind speed  $U^2$  is the  $U_{cr}^2$  that causes torsional divergence of the bridge.

### 2.1.2 Two-degree of freedom flutter

After several studies, the researchers found the possibility to adapt the analyses developed on the wings of the planes on the sections of suspension bridges to perform aeroelastic stability analyses.

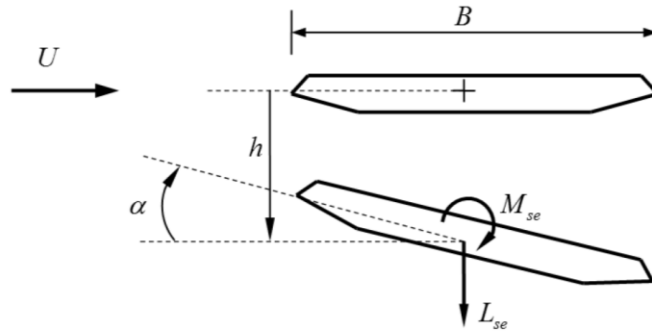


Figure 2-8: Two degrees of freedom simplify model

In their formulation, Scanlan and Tomko have shown that, in small fluctuations field, self-exciting forces assume expressions function of the coordinates  $h$  and  $\alpha$ :

$$L_{SE} = \frac{1}{2} \rho U^2 B \left[ KH_1^*(K) \frac{\dot{h}(t)}{U} + KH_2^*(K) \frac{B \cdot \dot{\alpha}(t)}{U} + K^2 H_3^*(K) \alpha(t) + K^2 H_4^*(K) \frac{h(t)}{B} \right] \quad (2-18)$$

$$M_{SE} = \frac{1}{2} \rho U^2 B^2 \left[ KA_1^*(K) \frac{\dot{h}(t)}{U} + KA_2^*(K) \frac{B \cdot \dot{\alpha}(t)}{U} + K^2 A_3^*(K) \alpha(t) + K^2 A_4^*(K) \frac{h(t)}{B} \right] \quad (2-19)$$

where:

- $t$ : time(s);
- $K = \frac{\omega B}{U}$ : fluctuating reduced frequency;
- $\omega$ : angular frequency of fluctuating [rad/s];
- $H_i^*(K), A_i^*(K)$ : flutter derivatives obtained in wind tunnel.

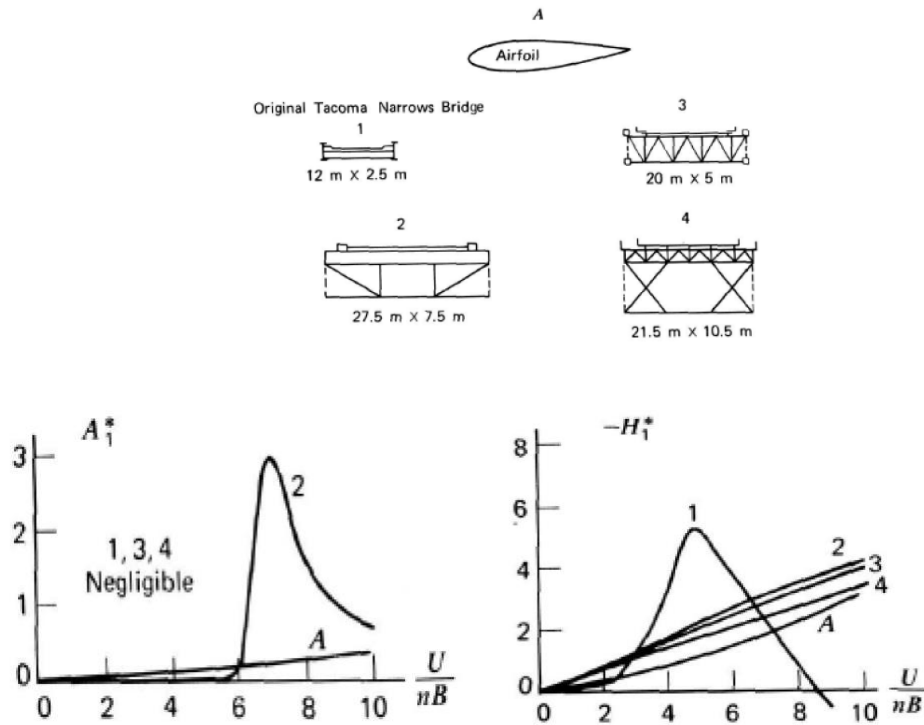


Figure 2-9: Examples of flutter derivatives

Classical formulation for flutter analysis starts from the hypothesis that the interaction between wind and structure can be evaluated using bi-dimensional calculation of transversal section of the deck, so tri-dimensional effects are negligible. Another simplification is to neglect section motion in wind direction. So, it is possible to consider two degrees of freedom in the bridge section that are vertical translation, defined by  $h$  displacement, and rotation  $\varphi$ .

The equations of motion can be expressed in these forms:

$$m\ddot{h}(t) + c_h\dot{h}(t) + k_h h(t) = L_{SE}(t, K) \quad (2-20)$$

$$I\ddot{\alpha}(t) + c_\alpha\dot{\alpha}(t) + k_\alpha\alpha(t) = M_{SE}(t, K) \quad (2-21)$$

- $m$ : is the mass of system for unit length;
- $I$ : is the deck polar moment of inertia for unit length;
- $c_h, c_\alpha$ : mechanic dumping factors;
- $k_h, k_\alpha$ : elastic stiffness factors.

$L_{SE}, M_{SE}$  characterize the force in orthogonal direction respect to wind speed and aerodynamic moment on the section. These terms, in a flutter analysis, depend on section bridge displacement.

Generally, aerodynamic forces are related to the reduced pulsation  $K$  with the Eq. 2-18, 2-19. Knowing the forces  $L_{SE}$ ,  $M_{SE}$ , the flutter critical wind speed can be obtained.

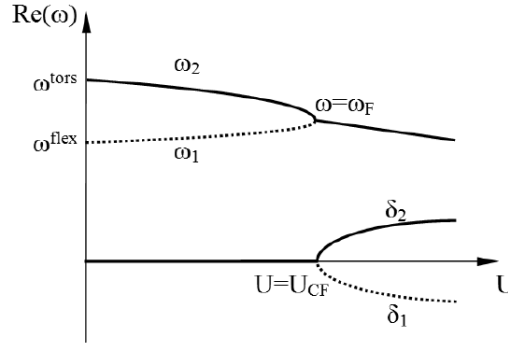


Figure 2-10: Definition flutter critic speed

It is necessary to search harmonic solution of the Eq. 2-20, 2-21 in the form:

$$h(t) = h_0 e^{i\omega t}; \alpha(t) = \alpha_0 e^{i\omega t} \quad (2-22)$$

By separating the real and imaginary parts, two equations of the 3<sup>th</sup> and 4<sup>th</sup> order in  $K$  are obtained. The common solution gives the reduced frequency for flutter  $K_F$ . The frequency  $\omega_F$  that satisfies the two equations is the flutter frequency.

So, the flutter instability speed can be obtained as:

$$U_F = \frac{B\omega_F}{K_F} \quad (2-23)$$

In non-conservative models, the system becomes instable when two pulsations, of flexural and torsional oscillations, are timed on the same frequency and become complex conjugates. In this case, an alternative equilibrium configuration for the structure doesn't exist. The case of two complex conjugates pulsations gives flutter instability phenomenon and the corresponding load is called the flutter load.

### 2.1.3 One-degree of freedom flutter

Considering stocky bridge sections, the influence of  $\alpha$  and  $\dot{\alpha}$  in  $L_{SE}$  and of  $h$  and  $\dot{h}$  in  $M_{SE}$  are negligible.

So, motion equations assume decoupled formulation:

$$m\ddot{h}(t) + c_h\dot{h}(t) + k_h h(t) = \frac{1}{2}\rho U^2 B \left[ KH_1^*(K) \frac{\dot{h}(t)}{U} \right] \quad (2-24)$$

$$I\ddot{\alpha}(t) + c_{\alpha}\dot{\alpha}(t) + k_{\alpha}\alpha(t) = \frac{1}{2}\rho U^2 B^2 \left[ KA_2^*(K) \frac{B \cdot \dot{\alpha}(t)}{U} + K^2 A_3^*(K)\alpha(t) \right] \quad (2-25)$$

In this case aero-elastic instability depends on self-exciting fluctuations in bending or torsion mode. Bending flutter is also called galloping.

Considering the torsional motion:

$$I\ddot{\alpha}(t) + c_{\alpha}\dot{\alpha}(t) + k_{\alpha}\alpha(t) = c_{\alpha}^*\dot{\alpha}(t) + k_{\alpha}^*\alpha(t) \quad (2-26)$$

And thus:

$$I\ddot{\alpha}(t) + (c_{\alpha} - c_{\alpha}^*)\dot{\alpha}(t) + (k_{\alpha} - k_{\alpha}^*)\alpha(t) = 0 \quad (2-27)$$

where:

$$c_{\alpha}^* = \frac{1}{2}\rho U^2 B^2 KA_2^*(K) \left( \frac{B}{U} \right) \quad (2-28)$$

$$k_{\alpha}^* = \frac{1}{2}\rho U^2 B^2 K^2 A_3^*(K) \quad (2-29)$$

are aerodynamic damping and aerodynamic stiffness factors.  $c_{\alpha}^*, k_{\alpha}^*$  are positive for positive  $A_2^*, A_3^*$ . If  $U$  increases, two configurations are possible:

- Global damping factor ( $c_{\alpha} - c_{\alpha}^*$ ) can assume value of zero or negative value; for  $(c_{\alpha} - c_{\alpha}^*) < 0$ , a trouble on the profile is amplified by energy transported from fluid to structure, if  $(c_{\alpha} - c_{\alpha}^*) = 0$  the fluctuation is harmonic.
- Global stiffness factor ( $k_{\alpha} - k_{\alpha}^*$ ) can assume value of zero or negative value; for  $(k_{\alpha} - k_{\alpha}^*) < 0$  instability aerodynamic moment is bigger than stability elastic one and a static instability is present.

Flutter condition and its critical speed are evaluated by:

$$c_{\alpha} - \frac{1}{2}\rho U^2 B^2 KA_2^*(K) \left( \frac{B}{U} \right) < 0 \quad (2-30)$$

It is possible to define the damping factor:

$$\zeta_{\alpha} = \frac{c_{\alpha}}{2I_{\alpha}\sqrt{\frac{K_{\alpha}}{I_{\alpha}}}} = \frac{c_{\alpha}}{2I_{\alpha}\omega_{\alpha}} \rightarrow c_{\alpha} = 2I_{\alpha}\omega_{\alpha}\zeta_{\alpha} \quad (2-31)$$

The Eq. 2-30 becomes:

$$2I_{\alpha}\omega_{\alpha}\zeta_{\alpha} - \frac{1}{2}\rho U^2 B^2 KA_2^*(K) \left( \frac{B}{U} \right) < 0 \quad (2-32)$$

For long span bridges, it is highlighted the empirical connection between  $A_2^* = A_2^*(K)$ . The imaginary part of the eigenvalue obtained on the motion *Eq. 2-25* is equal to pulsation  $\omega_\alpha$ , with good approximation.

It is possible to assume:

$$(A_2^*)_F = \frac{2I_\alpha \zeta_\alpha}{\rho B^4} \quad (2-33)$$

Using this formulation,  $K_F$  will be evaluated without iterative process, and thus the flutter critical speed can be obtained as:

$$U_F = \frac{\omega_\alpha B}{K_F} \quad (2-34)$$

# CHAPTER 3

## NUMERICAL FULL-BRIDGE MODELLING AND DESCRIPTION OF THE CASES STUDY

In the USA, when the *Wheeling Bridge* and the *Tacoma Narrow Bridge* fell down, started the analysis of wind effects on the design of big span bridges. In the last century and in the past years, different approaches have been developed by several authors with the goal of studying the behaviour of big span bridges under wind action.

Basically, there are two types of methods:

- The first one is more general, tested on ideal bridges and can be used for real structures.
- The other consists of a series of methods that have been developed for specific real problems. Even though it is focused on particular cases, this fact does not avoid applying the same procedure on other cases in order to verify the behaviour of suspension bridges.

The first phase consists in a modal analysis of the bridge to evaluate the natural frequencies of the structure and the related modal shapes. In the following step, a static approach starts in order to obtain the critical wind speed that causes the torsional divergences (described in *Chap. 2*).

The third phase considers a unsteady analysis to evaluate the flutter wind speed, that is the more dangerous phenomenon on suspension bridges due to the high slenderness of this kind of structures. Flutter analysis can be performed in time domain or in frequencies domain; considering the first case, it is possible to describe the displacements and the rotations of one

or more points of the deck for different wind speed, and, in case of divergence of one value, it is obtained flutter critic speed.

The frequencies domain approach, instead, is based on complex eigenvalues analysis where, for each wind speed, a critical mode is evaluated, considering real and imaginary part of the solution. The real part represents the frequency of critical mode and the imaginary one describes the stability of solution, or the opposite, and when it becomes equal to zero, there is the flutter phenomenon.

### 3.1 A Salvatori and Borri study

In 2007, Salvatori and Borri with the collaboration of “Università degli studi di Firenze”, presented a non-linear semi-empirical analysis performed on ideal suspension bridges where the deck has a rectangular cross section.

#### 3.1.1 Analysis method

A numerical framework for full-bridge aeroelasticity is presented, based on unsteady cross-sectional load models and on the finite elements modelling of the structure. A frequency-domain approach based on aeroelastic derivatives and nonlinear complex eigenvalue analysis is compared to its equivalent time-domain counterpart based on indicial functions and direct integration of the equations of motion.

Considering the *Figure 3-1*, a bridge with straight span subjected to a wind flow is considered, with a mean velocity horizontal and orthogonal to the bridge span. The bridge deck cross-section, in the  $xz$  plane, is treated as a rigid body. Hence, the motion of the cross-section is described by three degrees of freedom, respectively the horizontal displacement, the vertical displacement  $z$ , and the rotation  $\alpha_y$ .

The pressure field around the cross-section results in a horizontal force  $F_x$ , a vertical force  $F_z$  and a pitching moment  $M_y$ , power-conjugated with the rates of  $x$ ,  $z$ , and  $\alpha_y$  respectively.

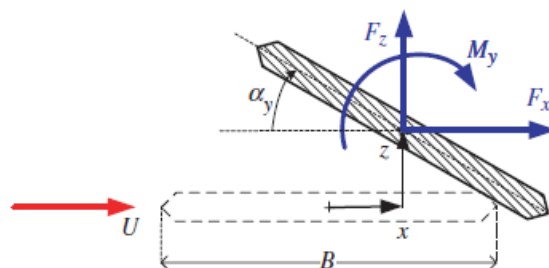


Figure 3-1: Forces acting on bridge section[5]

A typical ‘fishbone-like’ structural model is shown in *Figure 3-2*. Wind actions are applied through special one-node ‘elements’ characterized by an orientation and an along span influence length. The discretized equation of motion is presented as follow:

$$M\ddot{d} + C\dot{d} + F_k(d) = P_{dead} + P_{wind} \quad (3-1)$$

where:

- $d$ : is the vector of nodal degrees of freedom;
- $M$ : is the mass matrix;
- $C$ : is the linear dumping matrix;
- $F_k$ : is the vector of internal structural forces;
- $P_{dead}, P_{wind}$ : are the dead and wind load.

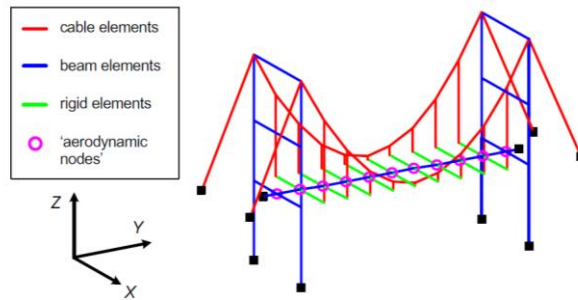


*Figure 3-2: Representation of discrete structural model*

For dynamic analyses, a model linearized around the mean steady configuration  $d$  is considered, where  $d$  is evaluated for each value of wind speed  $U$ . Now it is possible to obtain a linearized equation of motion:

$$M\ddot{\delta} + C\dot{\delta} + F_k(\delta) = P_a + P_b \quad (3-2)$$

where:

- $\delta=d-d'$ : is the vector of the displacements around the main steady configuration;
- $P_a, P_b$ : are the vectors assembling the self-excited aeroelastic forces and buffeting forces respectively.

Performing a frequency domain analysis, the vector of aeroelastic load is:

$$P_a^{AD} = -K_a^{AD}(U, \omega)\delta - C_a^{AD}(U, \omega)\dot{\delta} \quad (3-3)$$

where:

- $K_a^{AD}$ : is the matrix of flutter function in term of stiffness;
- $C_a^{AD}$ : is the matrix of flutter function in term of dumping.

Let  $\phi$  be the matrix whose columns are N selected mass-normalized modal shapes and considering  $\delta \sim \phi \zeta$ , the equations of motion are projected in a reduced modal shape.

$$\ddot{\zeta} + \phi^T(C + C_A)\dot{\zeta}\phi + \phi^T(K + K_A)\zeta\phi = 0 \quad (3-4)$$

Introducing  $\eta \sim \dot{\zeta}$ , the system is represented in the state space and reduced to a homogeneous system of first order differential equations.

$$\dot{\psi} = A\psi \quad (3-5)$$

where:

- A: is a matrix function whose terms are function of  $(K - K_a^{AD})$  and  $(C - C_a^{AD})$  (C and K structural dumping and stiffness), and  $\phi$ ;
- $\psi = [\eta^T \zeta^T]^T$ .

So, a non-linear complex eigenproblem it is obtained:

$$(A - \lambda I)\psi = 0 \quad (3-6)$$

in which:

- $\psi = [\eta_n^T \zeta_n^T]^T = [\lambda \eta_n^T \zeta_n^T]^T$ .

Each couple of conjugated eigenvalues can be written as  $\lambda_n = -\nu_n \omega_n \pm i \omega_n \sqrt{1 - \nu_n^2}$ , where  $\omega_n = \|\lambda_n\|$  is the circular frequency and  $\nu_n = -\frac{Re(\lambda_n)}{\omega_n}$  is the damping ratio and  $i$  the imaginary unit. The matrix A is a function of the frequency and each eigenvalue must be computed iteratively. To the purpose of this part analysing stability, we focus only on the lowest-damping mode, which is potentially responsible of instability. More in general, it is possible to repeat the nonlinear calculation for each mode; in this way the structural modes that were coupled by aeroelastic effects can be uncoupled again. This step allows frequency-domain buffeting analyses as shown in flow chart (*Figure 3-3*). The analysis starts with zero-mean wind velocity and an assumption on the frequency of the critical mode. Then  $U$  is increased step by step, for each one of which the mean steady configuration is evaluated, by non-linear analysis. After assembling matrix A and performed its spectral calculation, the

lowest damping eigenvalue is selected. The actual frequency is different respect to the trial one, so it is necessary to have an iterative calculation until convergence. The real part of the converged eigenvalue governs the stability of the system; if a positive damping is obtained,  $U$  is incremented and the old frequency is used as initial assumption for the next iterative loop.

The analysis ends as soon as non-positive damping is obtained, so critical speed is evaluated.

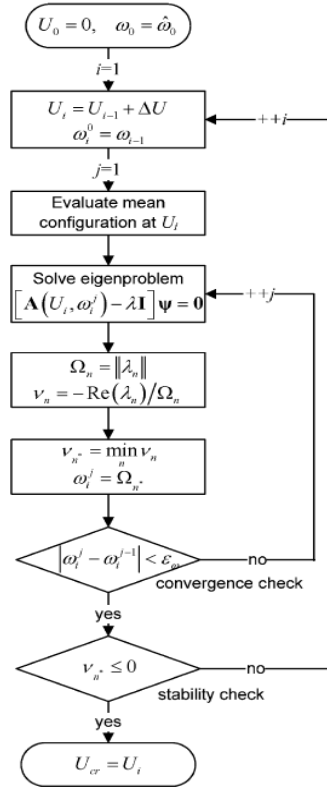


Figure 3-3: Flow chart of stability analysis in frequency domain

In time-domain, the linearized problem is:

$$M\ddot{\delta} + C\dot{\delta} + K\delta = P_a^{IF} = -K_a^{IF}\delta - C_a^{IF}\dot{\delta} + P_{conv}^{IF} \quad (3-7)$$

where:

- $P_a^{IF}$ : is a vector obtained from indicial functions depending by flutter derivatives;
- $K_a^{IF}, C_a^{IF}, P_{conv}^{IF}$ : assemble the contribution of each modelled cross-section.

The time integration of Eq. 3-7 is performed with trapezoidal rule, that is unconditionally stable for linear problems. When typical bridge characteristics are used, the

choice of the time-step size is dictated by the evaluation of the convolution integrals, so that no problem arises in the integration of the equations of motion. The computational efficiency can be improved by using a smaller timestep for the evaluation of the convolution integrals and a larger one for the integration of the equations of motion; in this case an interpolation scheme must be provided from the coarser to the finer time-discretization.

As sample structure an ideal suspension bridge with 1400 m main span and streamlined deck-aerodynamics is chosen. The main geometrical and mechanical characteristics of the structure are illustrated in *Figure 3-4*, and reported in *Table 3-1* (steel deck is assumed). The main span of the bridge is discretized with 20 elements.

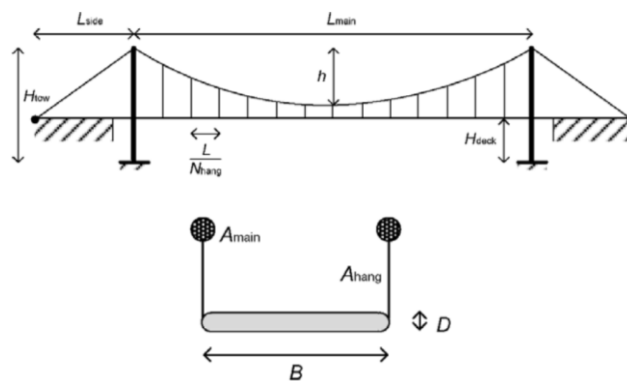


Figure 3-4: Geometry of the bridge

<b>Main span length</b>	$L_{Main}=1400.00$ m
<b>Side span length</b>	$L_{side}=320.00$ m
<b>Tower height</b>	$H_{tower}=190.00$ m
<b>Deck height above ground level</b>	$H_{deck}=60.00$ m
<b>Main cable sag</b>	$H=128.00$ m
<b>Number of hangers in the main span</b>	$N_{hang}=70$
<b>Deck width</b>	$B=35.00$ m
<b>Deck height</b>	$D=2.45$ m
<b>Main cable cross-section area</b>	$A_{main}=0.5500$ m <sup>2</sup>
<b>Hanger cross-section area</b>	$A_{hang}=0.0090$ m <sup>2</sup>
<b>Deck mass per unit-span</b>	$M_{deck}=14.0 \cdot 10^3$ kg/m
<b>Deck rotational mass per unit-span</b>	$\Theta_{deck}=1400 \cdot 10^3$ (kg m <sup>2</sup> )/m
<b>Deck cross-section area</b>	$A_{deck}=1.40$ m <sup>2</sup>
<b>Deck moment of inertia about X</b>	$J_{y,deck}=2.50$ m <sup>4</sup>
<b>Deck moment of inertia about Z</b>	$J_{z,deck}=145.00$ m <sup>4</sup>
<b>Deck torsional constant</b>	$J_{t,deck}=11.00$ m <sup>4</sup>

Table 3-1: Geometrical properties Salvatori-Borri bridge

### 3.1.2 Analysis results

Considering time-domain analysis, at each incremental step, the equations of motion are linearized around the mean steady configuration and the indicial function load model is considered. After the imposition of a perturbation as initial condition, it is possible to perform a direct-time integration of Eq. 3-7, then the history of motion is analysed. At sub-critical mean wind velocities, the oscillations are damped down (Figure 3-5a), whereas at super-critical mean wind velocities diverging oscillations appear. The borderline condition of stationary oscillations represents the critical stability threshold (Figure 3-5b) and is obtained for a mean wind velocity of 75.7 m/s. The relevant critical frequency of 0.241 Hz is computed through the Fourier analysis.

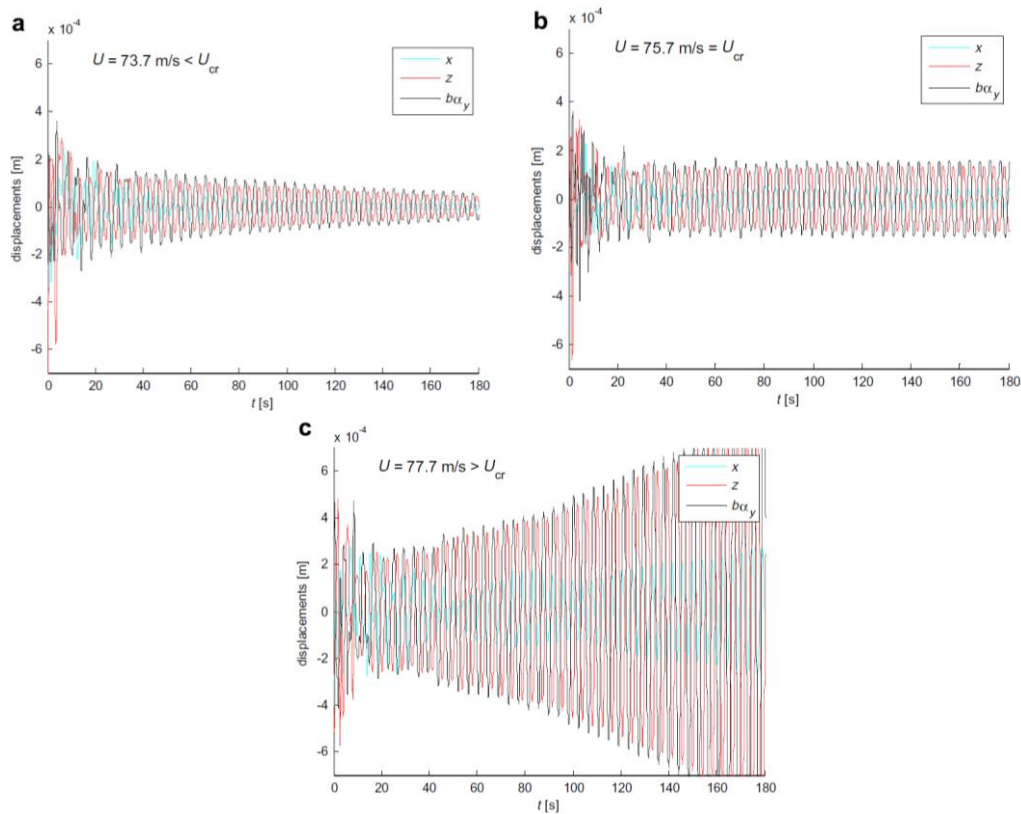


Figure 3-5: Time history fluctuations

The stability analysis in the frequency domain is performed according to the procedure described above. The present goal is the comparison with the time-domain simulations of the full structure. As first analysis, it is necessary to evaluate the aeroelastic stiffness and damping by using the approximation of unsteady coefficients. In this case the analysis is theoretically equivalent to the time-domain one based on identified indicial functions, as confirmed by the

numerical results which agree within the computational accuracy. A mode with non-positive damping is firstly obtained at a mean wind velocity of 75.8 m/s with a frequency of 0.236 Hz and the critical mode is a symmetric coupled vertical–torsional flutter.

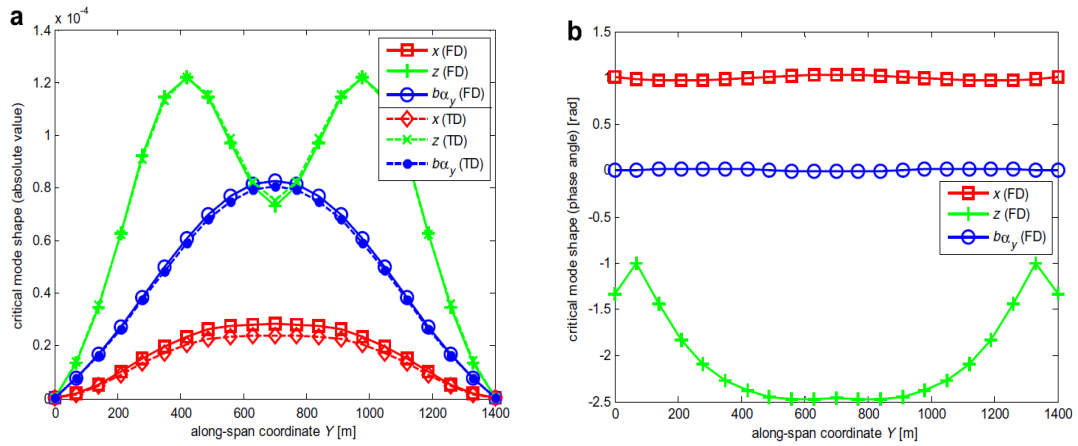


Figure 3-6: Critical mode-shape (absolute value on the left, phase angle on the right)

## 3.2 Akashi Kaikyo Bridge

This bridge over the Akashi Strait is one among several situated along the Kobe-Naruto route between the Japanese islands of Honshu and Shikoku. It crosses the Strait at a distance of about 4 km and connects Honshu, Japan’s main island, to neighbouring Awaji. The waterway is among the most navigated ones in the world, in fact maritime traffic is an important consideration. For the design, a suspension bridge was chosen with an extremely rigid latticework deck so that the Strait could be crossed using the minimum number of supports. Its total length is 3910 m, with a main span of 1991 m. Its two towers are 297 m high; crossbeams have been used as a reinforcement.

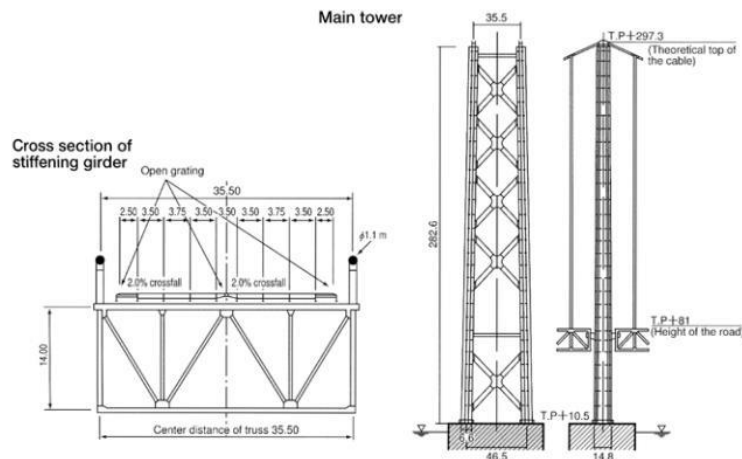


Figure 3-7: Akashi Kaikyo Bridge section

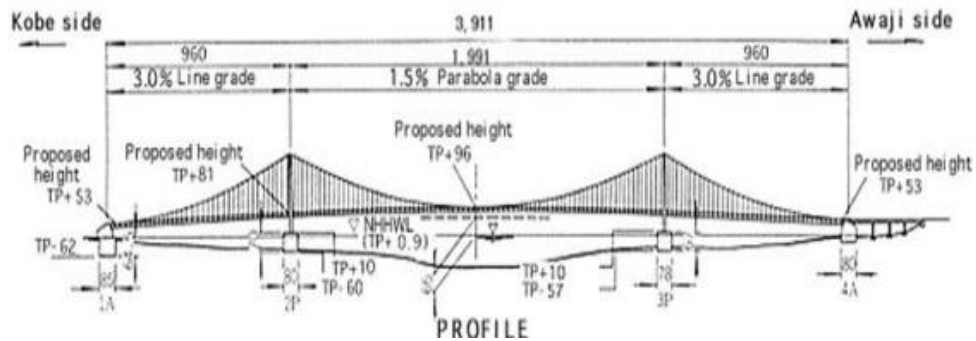


Figure 3-8: Akashi Kaikyo Bridge profile

Because of the high possibility of being hit by typhoons, rigorous tests have been carried out to ensure an appropriate response from the bridge when exposed to wind loads. Among all the most remarkable of these studies is the one carried out by Katsuchi at the *John Hopkins University*. Others include the experimental testing on a full model of the bridge on a scale of 1/100, done by Miyata.

<b>Main span length</b>	1991 m
<b>Lateral span length</b>	960 m
<b>Towers height</b>	297 m
<b>Number of hangers</b>	112 each side
<b>Total deck width</b>	35.5 m
<b>Distance between hangers</b>	17.75 m
<b>Deck edge</b>	14 m
<b>Diameter of main cables</b>	1.12 m
<b>Diameter of hanger</b>	0.19 m

<b>Deck moment of inertia about Y</b>	24 m <sup>4</sup>
<b>Deck moment of inertia about Z</b>	130 m <sup>4</sup>
<b>Torsion deck moment of inertia</b>	17.8 m <sup>4</sup>
<b>Deck mass</b>	28.7 tons/m
<b>Polar inertia moment in deck</b>	5800 (tons m <sup>4</sup> )/m

Table 3-2: Geometrical and mechanical properties of the Akashi Kaikyo Bridge

### 3.2.1 Miyata and Katsuchi studies

First of all, it is necessary to evaluate both the natural frequencies and modes for the *Akashi Kaikyo Bridge*. It is possible to obtain results by different approaches: Katsuchi studied the problem with an analytic approach as described in *Chap. 2*, Miyata analysed the bridge behaviour using a scale model 1/100 in a wind tunnel (*Figure 3-9*). Another possible approach is using the finite element software ADISNOL3D, where the numerical model of the bridge is realised with a “Fish-bone” structure (*Figure 3-10*).



Figure 3-9: Scale model used by Miyata

Another factor considered, using finite elements software, was the geometric non-linearity in the cable system.



Figure 3-10: Fish bone model used in ADISNOL3D

Table 3-3 compares the natural frequencies obtained by the different methods mentioned above.

Mode type	ADISNOL3D	KATSUCHI	MIYATA
<b>(1)H-S</b>	0.045	0.038	0.038
<b>(2)V-S</b>	0.0662	0.0652	0.0637
<b>(3)V-A</b>	0.0736	0.075	0.074
<b>(4)V-A</b>	0.085	0.085	0.083
<b>(5)H-A</b>	0.0946	0.0783	0.775
<b>(6)V-S</b>	0.122	0.121	0.121
<b>(10)L-TS</b>	0.158	0.127	0.149
<b>(11)V-S</b>	0.162	0.163	-
<b>(12)T-LS</b>	0.163	0.155	-
<b>(14)V-A</b>	0.174	0.171	-
<b>(24)T-A</b>	0.219	0.211	0.207
<b>(25)V-S</b>	0.227	0.221	-
<b>(26)T-A</b>	0.239	0.254	-
<b>(27)H-A</b>	0.25	0.221	-
<b>(28)T-S</b>	0.261	0.297	-
<b>(29)V-A</b>	0.282	-	-
<b>(38)T-S</b>	0.321	-	-

Table 3-3: Comparison of natural frequencies[6]

### ***Flutter analysis***

In the *Akashi Kaikyo Bridge*, an aeroelastic analysis using the 16 modes was chosen, based on multimodal theory. The flutter derivatives for the deck of this bridge were the ones used by Katsuchi in his own study on the bridge's aeroelastic behaviour. It is worth mentioning that the researcher also used for the study of this bridge the coefficients  $P_i$  ( $i = 1....6$ ) relating the force of horizontal thrust  $D$  (drag) to deck movements. According to the conclusions of Katsuchi, these coefficients have a marked influence on the bridge's behaviour under the phenomenon of flutter.

Using the finite elements software FLAS, the first step in studying the behaviour of the *Akashi Kaikyo Bridge* was to consider the two classic modes in flutter phenomena: the first mode of vertical bending and the first one of torsion. It must be remembered that in this bridge the first torsional modes also have an appreciable component of lateral bending. Tests were carried out on the two possibilities. The results are that when modes 2 and 10 are considered,

flutter does not occur until speeds of more than 100 m/s are reached. By contrast, if modes 2 and 12 are chosen, flutter is produced at 77.69 m/s, a more probable result. The graphical representations found in *Figure 3-11* underline the evolution of the real and imaginary parts of the eigenvalues obtained for the increasing wind speeds, as well as the critical wind speed values and the reduced frequency associated with it. As can be detected in the *Figure 3-11*, mode 12 of symmetrical torsion, with a noticeable lateral component, is responsible for the flutter instability, reached at a wind speed of  $U = 77.69$  m/s, and a reduced frequency of  $K = 0.4554$  corresponding to  $f = 0.158$  Hz.

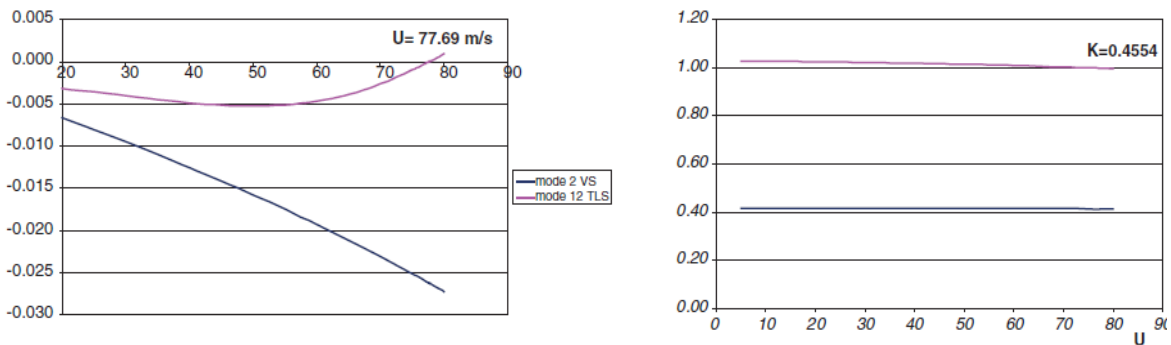


Figure 3-11: Real parts(left) and imaginary part (right) behaviour for 2 mode analysis[6]

It is possible to appreciate that the finite elements software used for this analysis doesn't present a stability on the solution with the increasing of natural modes analysed. In fact, using 17 vibration modes, FLAS software obtain the same kind of graphs used for the two-modes calculation.

The critical wind speed is  $U = 93.33$  m/s with  $K = 0.5064$  and  $f=0.175$  Hz. By observing *Figure 3-12*, one can see how, in this analysis, the factor responsible for flutter is mode 24, which is the one for asymmetric torsion (AT). Therefore, the mode in which null damping is reached within the two-mode analysis undergoes a variation (*TLS mode 12*).

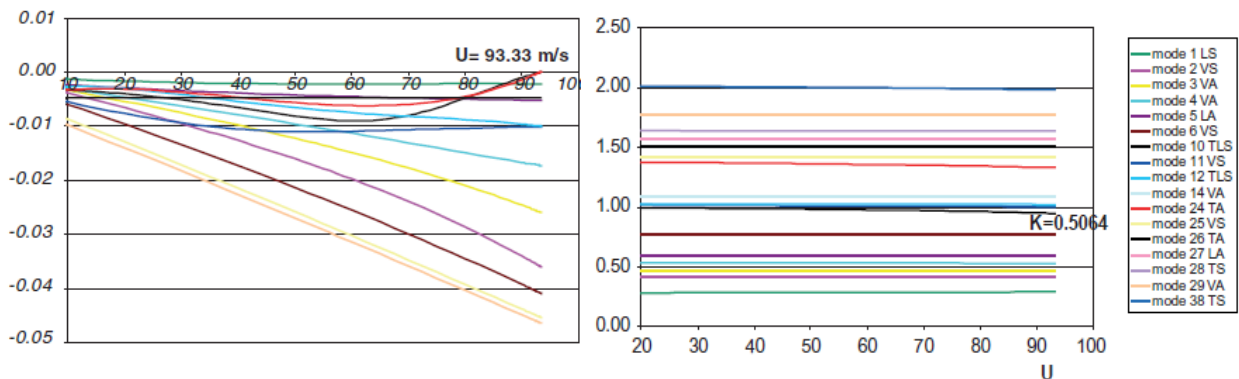


Figure 3-12: Real parts(left) and imaginary part (right) behaviour for 17 mode analysis[6]

Another considerable change takes place when the flutter speed increases more than 15 m/s. These differences invalidate the aeroelastic analysis carried out with two vibration modes on the Akashi Strait Bridge. Thus, it seems that, with any bridge with a main span over 1500 m long, an analysis based on two modes of vibration, using FLAS, could provide unreliable results.

Analysis	Flutter speed U (m/s)	Frequency f (Hz)
<b>FLAS, 2 modes</b>	77.69	0.157
<b>FLAS, 17 modes</b>	93.33	0.175
<b>Katsuchi, 2 modes</b>	58.9	-
<b>Katsuchi, 15 modes</b>	87-96	0.146
<b>Miyata (reduced model)</b>	85-95	0.207

*Table 3-4: Comparison of different flutter analysis[6]*

*Table 3-4* compares the results from the aeroelastic analyses carried out on the *Akashi Kaikyo Bridge* with the analytical calculations made by Katsuchi and the testing done by Miyata using a full model on a 1/100 scale. Drawing one's attention to the multimodal analyses, much more precise than those which use only two vibration modes, it is possible to observe how all the values in the table hover around 90 m/s, returning to more or less the same point according to the suppositions one makes. As for the response frequency, the value obtained by Katsuchi approximates one of the possibilities found in the analysis for 17 modes. On the other hand, the value obtained by Miyata in the reduced scale model study of the bridge is similar to the frequency of the other flutter shape.

### 3.2.2 D'Argenio study

The aeroelastic analysis of *Akashi Kaikyo Bridge* can be performed using analytic development, with the software MATLAB. In his Master's Thesis, D'argenio realised a program developed in MATLAB to study the behaviour of the bridge under wind effects.

Due to the fact that the effects given by the lateral spans of 960 m are not negligible, it is necessary to consider a reduced elastic modulus  $E^*=1.6E+10$  for the main cables to take into account the deformability of the piers under loads.

$\rho_a$	1.25 kg/m <sup>3</sup>	Air density
$C_d$	0.421	Aero-dynamic resistance factor
$C'_m$	0.306	Derivate of moment factor

*Table 3-5: Aero-dynamic properties of Akashi Kaikyo Bridge*

With aerodynamic and mechanical properties shown in *Table 3-3,3-5*, considered with angle of attach equal to zero, MATLAB software gives curves that represent the evolution with wind speed of frequencies of oscillation of the bridge (*Figure 3-13*) and corresponding modes (*Table 3-6*). Critic speed for the static instability is  $U_{cr}=108$  m/s.

The speeds for torsional divergences and flexural-torsional instability corresponding to critical loads  $p_{sc1}, \mu_{sc1}$  (*Eq. 2-6,2-8*) are:

- $U_{cr}=268.63$  m/s for antisymmetric torsional divergence;
- $U_{cr}=112.86$  m/s for antisymmetric flexural-torsional divergence;
- $U_{cr}=156.98$  m/s for symmetric torsional divergence;
- $U_{cr}=144.98$  m/s for symmetric flexural-torsional divergence;

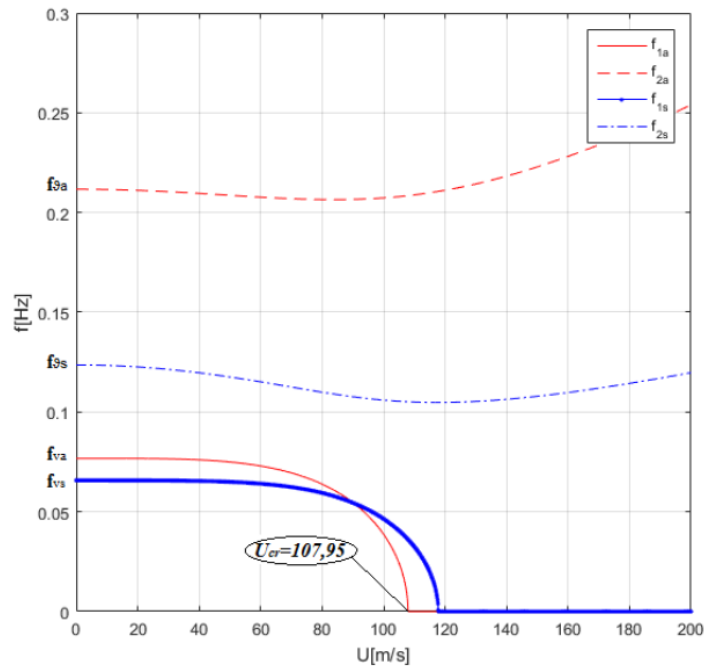


*Figure 3-13: Flexural and torsional frequencies behaviour respect wind speed, of Akashi Kaikyo Bridge, obtained with MATLAB*

Mode	Frequency (Hz)
<b>1<sup>st</sup> H-S</b>	0.027
<b>1<sup>st</sup> V-S</b>	0.066
<b>2<sup>nd</sup> H-A</b>	0.075
<b>1<sup>st</sup> V-A</b>	0.077
<b>2<sup>nd</sup> V-S</b>	0.120

<b>1<sup>st</sup>T-S</b>	0.124
<b>2<sup>nd</sup>V-S</b>	0.164
<b>1<sup>st</sup>T-A</b>	0.212

*Table 3-6: Natural frequencies of Akashi Kaikyo Bridge obtained with MATLAB program[7]*

D'Argenio's analysis, in order to evaluate the flutter speed, considers two unsteady aeroelastic actions, lift and moment (Eq. 2-18, 2-19), with second order effects. It is possible to write the expressions of  $L_v, M_\theta$  as functions of wind speed  $U$  and reduced wind speed  $U_r$ , considering the reduced frequency  $K = \frac{2\pi}{U_r}$ .

Now Eq. 2-18, 2-19 can be written as functions of four factors:

$$L_v = L_1 \left( \frac{\partial v}{\partial t} \right) + L_2 \left( \frac{\partial \theta}{\partial t} \right) + L_3 \theta + L_4 v \quad (3-8)$$

$$M_\theta = M_1 \left( \frac{\partial v}{\partial t} \right) + M_2 \left( \frac{\partial \theta}{\partial t} \right) + M_3 \theta + M_4 v \quad (3-9)$$

where:

- $L_i, M_i$ : are functions of flutter derivates obtained in the wind tunnel;
- $v$ : is the vertical displacement;
- $\theta$ : is the rotation.

The iterative procedure, used to obtain the flutter critical speed, starts with the definition of an initial  $U$  and  $U_r$  where flutter derivates are evaluated. It is possible to consider increasing values of two variables and for each one of  $L_v, M_\theta$ , that are used to solve the eigenvalue problem on MATLAB software. Each eigenvalue  $\omega$  is composed by real and imaginary parts given by unsteady actions, and it defines the stability of the solution.

In fact, when the imaginary part becomes negative, the critical value  $U_{r,crj}$  is obtained; the real part represents the critical value of pulsation  $\omega_{cr,j}$ . This value must be compared with analytic result  $\omega_j = \frac{2\pi U_j}{U_{rcrj} B}$ , using the wind speed assumed at the beginning of iterative cycle  $j$ . The iteration stops when the difference between  $\omega_j, \omega_{cr,j}$  is smaller than the tolerance (0.01-0.03). The wind speed value for which convergence is reached, it will be the critical flutter speed  $U_f$ . One result is obtained for the symmetric modes and another one for the anti-symmetric modes, the smallest one is the correct instability value.

Akashi Kaikyo Bridge	$U_{rc}$	$f_c$ [Hz]	$U_f$ [m/s]
<b>Anti-symmetric configuration</b>	29.397	0.0791	81.1
<b>Symmetric configuration</b>	28.454	0.0660	65.1

Table 3-7: Critic flutter wind speed and frequencies for symmetric and anti-symmetric configurations, with second-order effects[7]

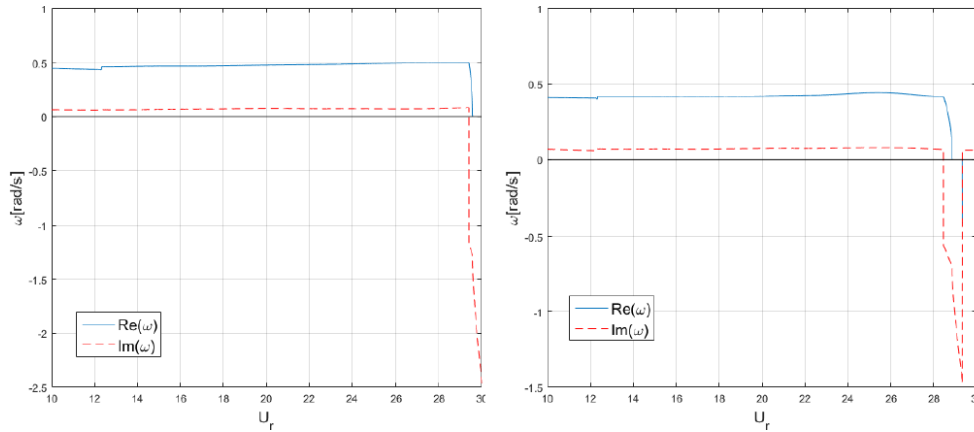


Figure 3-14: Solutions for individuation of critic flutter speed with second-order effects: anti-symmetric mode (left), symmetric mode (right)

Akashi Kaikyo Bridge	$U_{rc}$	$f_c$ [Hz]	$U_f$ [m/s]
<b>Anti-symmetric configuration</b>	29.607	0.0748	77.0
<b>Symmetric configuration</b>	28.735	0.0637	63.4

Table 3-8: Critic flutter wind speed and frequencies for symmetric and anti-symmetric configurations, without second-order effects

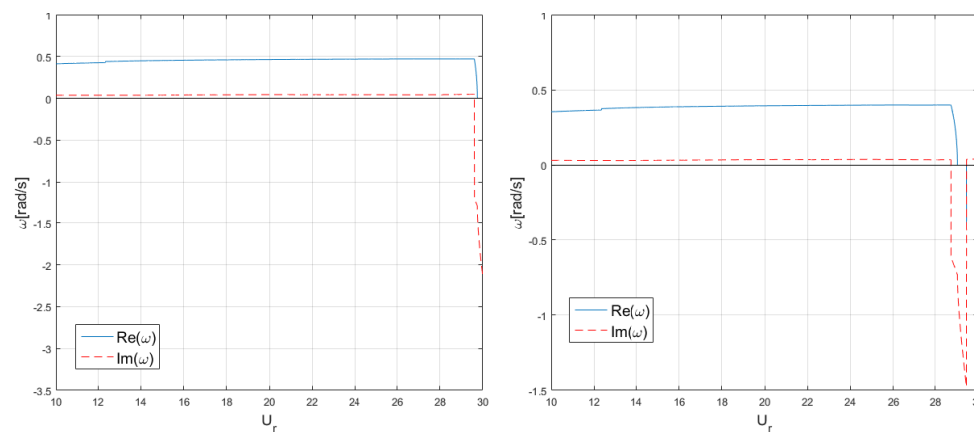


Figure 3-15: Solutions for individuation of critic flutter speed without second-order effects: anti-symmetric mode (left), symmetric mode (right)[7]

### 3.2.3 Maldera study: series of functions

The first step of this approach, performed by Maldera, is to evaluate the critic wind that causes static instability of *Akashi Kaikyo Bridge*. Using a flow developed in MATLAB, with the mechanical properties shown in *Table 3-2,3-5*, it is possible to obtain the critic value  $U_{cr} \cong 108 \text{ m/s}$  (*Figure 3-16*), as obtained in D'Argenio's thesis.

The program realised in MATLAB gives the curves of the oscillation frequencies respect to the wind speed. The graph gives a first value of the possible classical flutter critic speed, that is appreciable for a  $U_{cr} \cong 82 \text{ m/s}$ , where vertical and torsional motion become timed on the same frequency ( $f_{cr} \cong 0.1 \text{ Hz}$ ), that is the average value between the two fluctuations.

It is possible consider a two-degree of freedom analysis, vertical displacements  $v$  and the rotations  $\theta$ . The expression regarding the flexural and torsional behaviour of suspension bridges subjected to vertical load  $p(z)$  and torque moment  $m(z)$  are:

$$EI \frac{d^4 v}{dz^4} - H \frac{d^2 v}{dz^2} = p - \left(\frac{q_g}{H}\right)^2 \frac{E_c A_c}{l} \int_0^l v dz \quad (3-10)$$

$$EI_\omega \frac{d^4 \theta}{dz^4} - (GI_t + Hb^2) \frac{d^2 \theta}{dz^2} = m - b^2 \left(\frac{q_g}{H}\right)^2 \frac{E_c A_c}{l} \int_0^l \theta dz \quad (3-11)$$

where:

- $l$ : main span of the bridge;
- $b$ : half width of the deck;
- $q_g$ : self-weight of the bridge per unit span;
- $H$ : horizontal forces on main cables given by self-weight;
- $E_c A_c$ : extensional stiffness of main cables (constant value);
- $EI$ : flexural stiffness of the deck (constant value);
- $GI_t$ : principal torsional stiffness of section (constant value);
- $EI_\omega$ : secondary torsional stiffness (constant value).

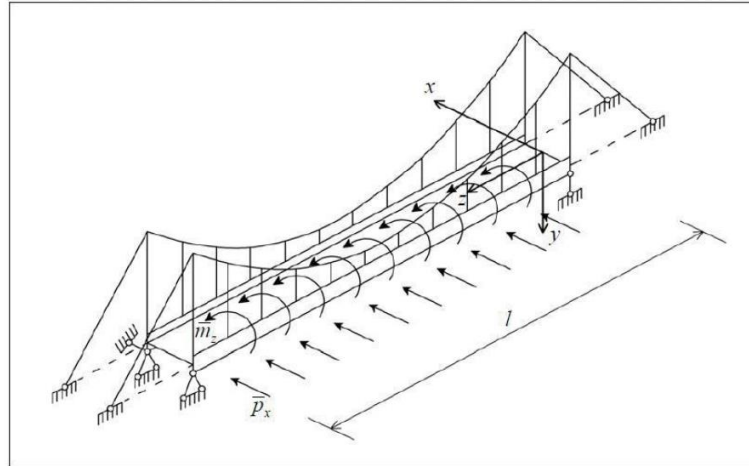


Figure 3-16: Main span of suspension bridge subjected to steady actions  $p_x, m_z$

Considering the deck in horizontal position and the wind load acting as shown in Figure 3-16, the aerostatic actions are evaluated as in Eq. 2-6,2-8, considering angle of attack  $\theta = 0$ . The stationary lift forces are negligible because of the huge loads of the bridge.

In case of symmetric oscillations, the integrals  $\int_0^l v dz$  and  $\int_0^l \theta dz$  in Eq. 3-10, 3-11 are equal to zero, and it is possible to insert the expressions of  $p_x, m_z$  in the same equations to study vertical and torsional behaviour of the deck.

The solution of the system defined by Eq. 3-10,3-11 can be looked for in the following form in separable variables:

$$v(z, t) = V(t)\eta(z); \quad \theta(z, t) = \phi(t)\psi(z) \quad (3-12)$$

where the functions  $\eta(z)$  and  $\psi(z)$  satisfy boundary conditions:

$$\eta(0) = \eta(l) = \frac{d^2}{dz^2} \eta(0) = \frac{d^2}{dz^2} \eta(l) = \psi(0) = \psi(l) = 0 \quad (3-13)$$

It is possible assume the following expression:

$$\eta(z) = \psi(z) = \sin \frac{2n\pi z}{l} \quad (3-14)$$

where:

- $n$ : natural number;
- *factor 2*: is necessary for selecting anti-symmetric deformed shapes only.

By inserting the solution given by Eq. 3-12 into the modified Eq. 3-10, 3-11, and a system of equation in matrix form is obtained:

$$[M]\{\ddot{q}\} + [K]\{q\} - p_x[K_g^p]\{q\} - \mu_s[K_g^\mu]\{q\} = \{0\} \quad (3-15)$$

The non-trivial solution can be found by the eigenvalues problem:

$$\det([K] - p_x[K_g^p] - \mu_s[K_g^\mu] - \omega^2[M]) = 0 \quad (3-16)$$

where:

- $\omega^2$ : are the dynamic eigenvalues of the system;
- $[K_g^p]$ : is the geometric stiffness matrix with respect to horizontal actions;
- $[K_g^\mu]$ : is the geometric stiffness matrix with respect to torque actions.

For each  $n$ , critic values of the transversal distributed load and distributed moment, that cause flexural-torsional instability and pure torsional divergence, are obtained. In the opposite case, with  $p_x = \mu_s = 0$ , natural pulsations are obtained.

Another important feature is the study of symmetric oscillations of the suspension bridge considering additional horizontal loads in the main cables in the Eq. 3-10, 3-11:

$$h_s(t) = \frac{q_g E_c^* A_c}{H l} \int_0^l [v(z, t) - b\theta(z, t)] dz \quad (3-17)$$

$$h_D(t) = \frac{q_g E_c^* A_c}{H l} \int_0^l [v(z, t) - b\theta(z, t)] dz \quad (3-18)$$

In the same way of the preceding case, the three-parameter model has a solution in the same separable variables form. In this case the expressions  $\eta(z), \psi(z)$  are defined by a series of sinusoidal functions:

$$\eta(z) = \psi(z) = a_1 \sin \frac{\pi z}{l} + a_3 \sin \frac{3\pi z}{l} + \sin \frac{5\pi z}{l} + \dots \quad (3-19)$$

where each coefficient  $a_i$  is determined from the free oscillations of the bridge. In this case mode-shape  $n$  will be defined by a series of  $a_i$  factors, that give their contribution to define the modal shape. The analysis gives a good solution using only the first four terms in  $\eta(z), \psi(z)$  expressions.

By substituting  $\eta(z), \psi(z)$  in to Eq. 3-10, 3-11, modified for symmetrical approach, the eigenvalues-eigenvectors problem is obtained.

In this case, it is possible to observe that if  $\eta(z), \psi(z)$  are defined by four factors, the matrix  $[K_g^p]$  loses its symmetry because some additional term appears.

Considering *Akashi Kaikyo Bridge* and approximating  $\eta(z) = \psi(z)$  with a series of four functions, the increase in stiffness results very small. In fact, it is possible to evaluate a rise of  $U_{cr}$  for torsional divergence and flexural-torsional symmetric instability of 2.9% and 0.8% respectively.

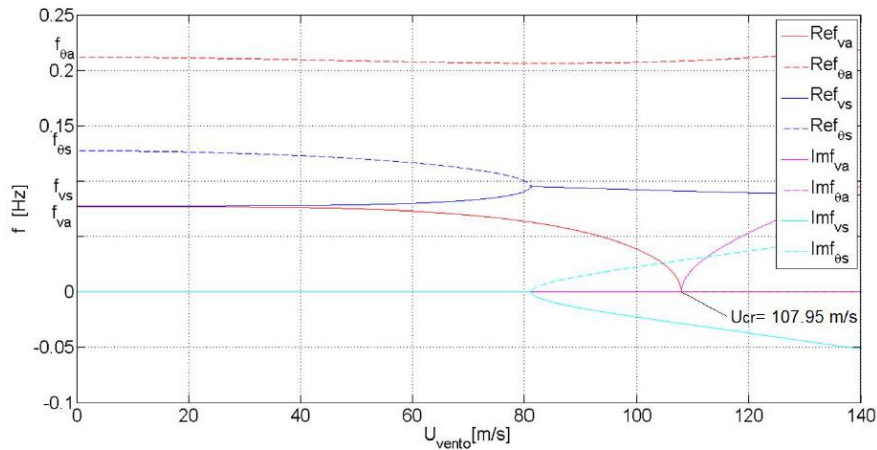


Figure 3-17: Flexural and torsional, real and imaginary part behaviour respect wind speed, of *Akashi Kaikyo Bridge*, obtained with MATLAB, one approximating function[8]

Considering no wind loads it is possible to evaluate natural frequencies of vibration with four approximating functions (Table 3-9).

Mode	Frequency [Hz]
<b>1<sup>st</sup> V-A</b>	0.0767
<b>1<sup>st</sup> V-S</b>	0.0776
<b>1<sup>st</sup> T-S</b>	0.1237
<b>1<sup>st</sup> T-A</b>	0.2117

Table 3-9: Natural frequencies of *Akashi Kaikyo Bridge* obtained with four-function analysis

The analysis of variation of vibration frequencies, respect to the wind speed, is developed using four function approximation. The new graph highlights an increasing of flexural and torsional frequencies of 19% and 3% respectively. The low influence in torsional frequencies depends by the huge torsional stiffness of the deck of *Akashi Kaikyo* (Figure 3-18).

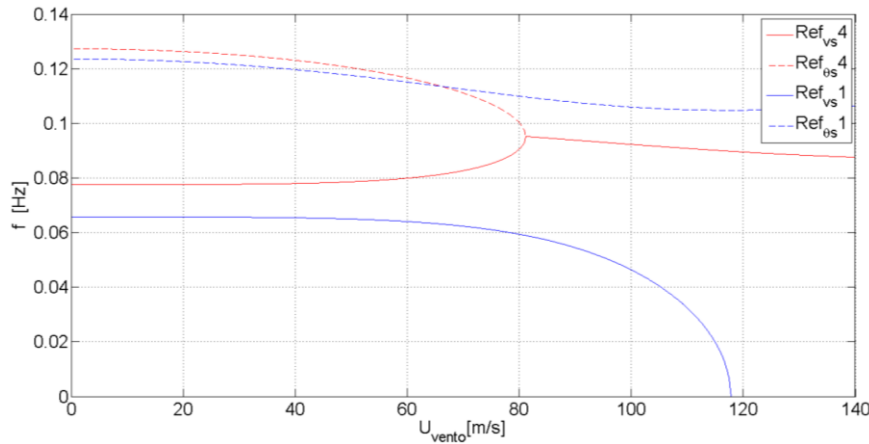


Figure 3-18: Behaviour of torsional and flexural frequencies respect wind speed, obtained with one and four approximating functions[8]

It is possible to consider that aerodynamic stiffness is generally very small compared to the structural stiffness of the bridge, except for the stiffness related to the torsional rotation  $\theta$ . So, in the formulation of unsteady aeroelastic forces, the functions depending by  $H_4^*, H_5^*, H_6^*, A_4^*, A_5^*, A_6^*$  are negligible and Eq. 2-18,2-19 can be write as:

$$L_{ns} = \frac{1}{2} \rho U^2 B \left[ KH_1^*(K) \frac{\dot{v}}{U} + KH_2^*(K) \frac{B \cdot \dot{\theta}}{U} + K^2 H_3^*(K) \theta \right] \quad (3-20)$$

$$M_{ns} = \frac{1}{2} \rho U^2 B^2 \left[ KA_1^*(K) \frac{\dot{v}}{U} + KA_2^*(K) \frac{B \cdot \dot{\theta}}{U} + K^2 A_3^*(K) \theta \right] \quad (3-21)$$

With the same procedure used by D'Argenio (*Chap. 3-3-2*) in MATLAB for symmetric and anti-symmetric cases, the flutter wind speed is evaluated considering four approximating functions to describe vertical displacements and torsional rotations of the deck.

Akashi Kaikyo Bridge	$U_{rc}$	$f_c$ [Hz]	$U_f$ [m/s]
<b>Anti-symmetric configuration</b>	29.6071	0.0743	81.1
<b>Symmetric configuration</b>	28.3593	0.0746	75.6

Table 3-10: Flutter critic speeds with second-order effects, using four approximating functions[8]

Akashi Kaikyo Bridge	$U_{rc}$	$f_c$ [Hz]	$U_f$ [m/s]
<b>Anti-symmetric configuration</b>	29.3977	0.0791	81.4
<b>Symmetric configuration</b>	28.0069	0.0760	77.2

Table 3-11: Flutter critic speeds without second-order effects, using four approximating functions[8]

It is possible to observe that considering second-order effects causes a reduction of flutter critic speed of 2.1% in symmetric configuration. In both cases (with and without second-order effects), the critical condition is obtained for the symmetric configuration.

<b>Symmetric configuration</b>	<b>4 sinusoidal functions <math>U_f</math> [m/s]</b>	<b>1 sinusoidal function <math>U_f</math> [m/s]</b>	<b>% relative error</b>
<b>2<sup>nd</sup> order analysis</b>	75.6	65.1	16
<b>Standard analysis</b>	77.2	63.4	21

*Table 3-12: Results with second-order and standard analysis, with four and one approximating functions*

## **PART 2**

# CHAPTER 4

## TEST PROBLEMS IN ANSYS

In **Part 1**, the historical development of the design and construction of suspension bridges, from 19<sup>th</sup> century until today, was discussed. At the beginning, the bridges were designed without considering in the appropriate way wind effects: several bridges, as *Tacoma Bridge* (1940), fell down for this reason. After this disaster, a new impulse in this direction arose, with studies on aerodynamics of bridges and analyses on aircraft wing, which were used for big span bridges applications to evaluate the actions of wind on the deck. In fact, it has been demonstrated that the wind effects are necessary to design suspension bridges. These structures, with their important length and slenderness, are very sensitive to the horizontal loads that could cause important flexural and torsional displacements.

In *Chap. 2*, it has been shown that the most dangerous phenomenon that may occur on suspension bridges is flutter, in fact when it emerges the consequences for the structure are catastrophic.

Wind effects analysis on bridges can be performed with different methods as shown in

**Part 1:**

- Analytic analysis;
- Finite elements numerical methods;
- Studying the behaviour of reduced model in wind tunnel.

In **Part 2** suspension bridges, in particular *Akashi Kaikyo Bridge*, will be studied by using the finite element software *ANSYS*. The results will be compared with those obtained in **Part 1** and those presented in the literature for this structure.

An important goal of the analysis is the validation of the analytic and numerical methods, in case of compatibility of results respect to bibliographic ones.

First, it will be necessary to analyse simple cases with software *ANSYS* to ensure the accuracy of the results obtained. After, it will be possible to study more complex structure and, in the end, a flutter analysis of the longest suspension bridge in the world, the *Akashi Kaikyo Bridge*, will be realised.

## 4.1 Dynamics of straight prestressed cable

The first case considered is a straight cable (*Figure 4-1*), where a modal analysis is performed using *ANSYS* software and the results will be compared with those obtained with FEM software *Lusas* and with analytic results.

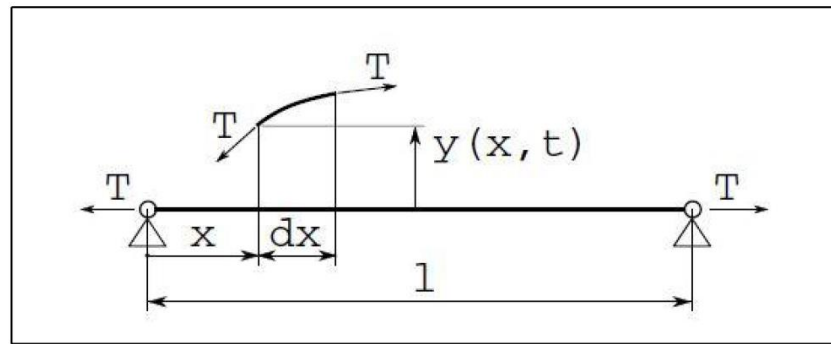


*Figure 4-1: Straight cable subjected to pretension T*

Consider the displacement  $y$  in orthogonal direction respect to  $x$ -axis, the equilibrium equation of a cable segment of length  $dx$  and mass  $\rho dx$  is:

$$\rho dx \frac{d^2 y}{dt^2} = -T \frac{dy}{dx} + T \left( \frac{dy}{dx} + \frac{d^2 y}{dx^2} dx \right) \quad (4-1)$$

It is possible to search a solution depending on  $x, t$ (time), in the form:

$$y(x, t) = \varphi(x)f(t) \quad (4-2)$$

And with the substitution of *Eq. 4-2* in *4-1*, it can be obtained:

$$\frac{1}{f(t)} \frac{d^2 f(t)}{dt^2} = \frac{T}{\rho} \frac{1}{\varphi(x)} \frac{d^2 \varphi(x)}{dx^2} \quad (4-3)$$

To verify *Eq. 4-3*, the two members must be equal to the same constant  $-\omega^2$ , and by solving the two separate differential equations they are obtained the infinite natural pulsations of the system:

$$\omega_i = i \frac{\pi}{l} \sqrt{\frac{T}{\rho}} \quad (4-4)$$

### 4.1.1 Numerical example

Now it is possible to perform a simple example of a tension straight cable, with the software ANSYS, with the properties of Table 4-1:

<b>Length</b>	30 m
<b>Cross section</b>	1.9 10 <sup>-4</sup> m <sup>2</sup>
<b>Pretension T</b>	30 kN
<b>Unit length weight</b>	1.5 kg/m

Table 4-1: Straight cable properties

First, in order to perform the FEM analysis, it is necessary to realise the numerical model in the software. The finite element that has been selected is BEAM188. It is a linear (2-node) beam element in 3D with six degrees of freedom in each node that includes translations in x, y and z directions and rotation respect to x, y and z axis. BEAM188 (Figure 4-2) includes stress stiffness terms, by default, in any analysis with the command *NLGEOM,ON*.

The element can be used with any cross section using the appropriate ANSYS command.

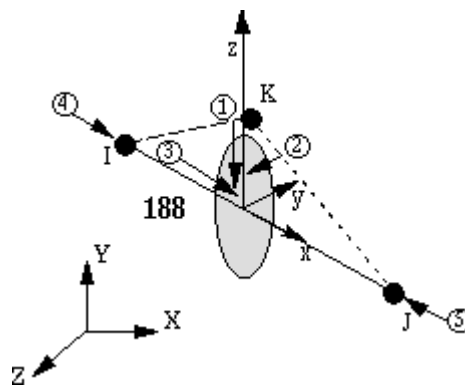


Figure 4-2: Representation of BEAM188 element[9]

The structure is simply supported in *xy* plane and only plane oscillations are considered. A concentrated load of 30 kN is applied; the mesh consists in 200 elements as in *Lusas* analysis.

Modal analysis is realised with the command *Solution>Analysis type>Modal* and selected *Analysis options>Block Lanczos* and *PSTRES,ON* to consider prestress effects.

Mode-shapes and relative frequencies are showed in *Figures 4-3;4-7*.



*Figure 4-3: Mode 1, 2.3595 Hz*

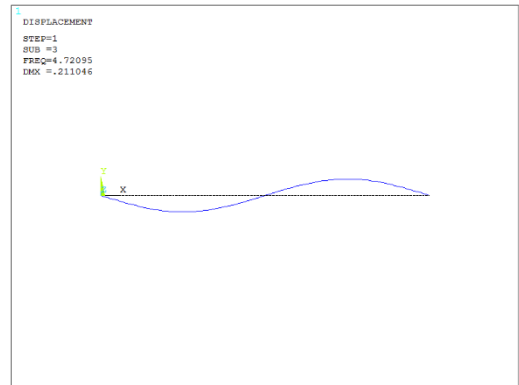


*Figure 4-4: Mode 2, 4.7209 Hz*



*Figure 4-5: Mode 3, 7.0865 Hz*



*Figure 4-6: Mode 4, 9.4581 Hz*

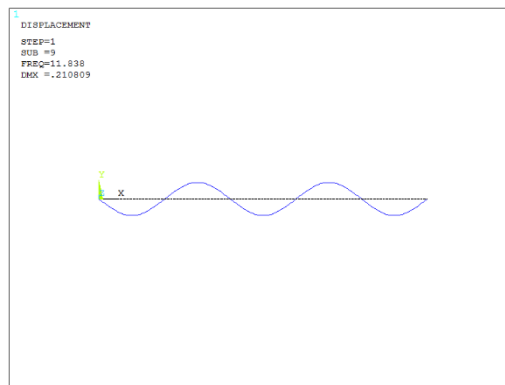


*Figure 4-7: Mode 5, 11.838 Hz*

The results obtained in *ANSYS* are now compared to *Lusas* and analytic ones and, for each mode, the relative error is evaluated to have an estimate of the accuracy of the numerical method.

Mode	Anslys frequency [HZ]	Lusas frequency [HZ]	Analytic frequency [HZ]	%err respect Lusas	%err respect analytic
1 <sup>st</sup>	2.3595	2.357	2.35	0.1	0.4
2 <sup>nd</sup>	4.7209	4.715	4.71	0.1	0.2
3 <sup>rd</sup>	7.0865	7.075	7.07	0.1	0.2
4 <sup>th</sup>	9.4581	9.438	9.43	0.2	0.3
5 <sup>th</sup>	11.838	11.805	11.78	0.3	0.5

Table 4-2: Results comparison and relative errors[10]

In Table 4-2, it is possible to observe as the differences in term of vibration frequencies are negligible, with a relative error smaller than 0.5% in both cases, and this is a first validation of the ANSYS numerical model.

## 4.2 Heavy cable small oscillations

Studying small oscillations of heavy cables is an important step to know the dynamic behaviour of suspension bridges. The dynamic behaviour of a cable is not linear because of the stiffening of the element, if the oscillation amplitude rises. It is possible to obtain a linearization of the problem considering small displacement of the heavy cable (Figure 4-8).

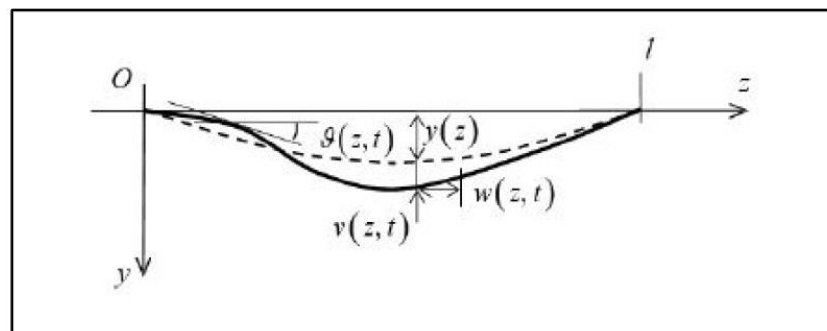


Figure 4-8: Heavy cable fluctuations

The dynamic equilibrium equations it is represented by:

$$H \frac{d^2 v}{dz^2} - \frac{h(t)}{H} q_g = \mu \frac{d^2 v}{dt^2} \quad (4-5)$$

where the pull action  $h$  is:

$$h(t) = \frac{EA q_g}{l H} \int_0^l v(z, t) dz \quad (4-6)$$

and:

- $H$ : is the horizontal component of the pull in the cable;
- $q_g$ : is the load given by self-weight for unit length on horizontal projection.

It is possible solve the problem with variable separation respect  $z$  coordinate and time  $t$ , and the solution of the Eq. 4-5 it is expressed as product of two functions:

$$v(z, t) = \eta(z)f(t) \quad (4-7)$$

Oscillations that satisfy the condition  $\eta(z) = -\eta(-z)$  are anti-symmetric and they don't cause variation of pull actions in the cable. The identity  $\eta(z) = \eta(-z)$  is relative to symmetric oscillations that cause an increase of pull actions.

Using the approach described in *Chap. 3.2.3* the natural pulsations are obtained for symmetric and anti-symmetric cases.

### 4.2.1 Numerical example

As in the previous case of a straight cable, it is possible to perform a modal analysis of the heavy cable with the software ANSYS. In this case there is also a validation of the numerical model for a problem with some peculiarities respect to the suspension bridge case.

In fact, it is possible to consider the heavy cable as the main cable of a suspension bridge that supports loads coming from the deck.

<b>Span</b>	1400 m
<b>Middle span displacement</b>	128 m
<b>Cross section</b>	0.55 m <sup>2</sup>
<b>E</b>	2E <sup>11</sup> N/m <sup>2</sup>
<b>Unit span weight</b>	221706 N/m

*Table 4-3: Geometrical properties of heavy cable*

The heavy cable, with the properties shown in *Table 4-3*, is realised in ANSYS using the element BEAM188 as in the case of straight cable, in *Chap 4.1*. The structure is subjected to self-weight actions that give its prestress. Hinges at the two ends allow rotation around  $z$  axis. The mesh consists in a discretization of 200 elements as in the same *Lusas* model. Performing modal analysis as described in the previous analysis, the following results can be obtained (*Figure 4-9;4-14*).

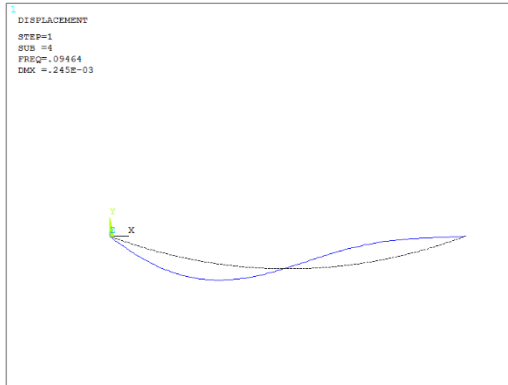


Figure 4-9: Mode 1 anti-symmetric, 0.09464 Hz



Figure 4-10: Mode 1 symmetric, 0.1323 Hz



Figure 4-11: Mode 2 anti-symmetric, 0.1937 Hz

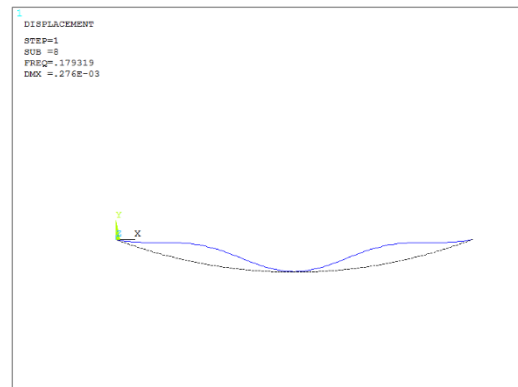


Figure 4-12: Mode 2 symmetric, 0.1793 Hz



Figure 4-13: Mode 3 anti-symmetric, 0.2918 Hz



Figure 4-14: Mode 3 symmetric, 0.2459 Hz

The results obtained in *ANSYS* are now compared to *Lusas* and analytic ones and, for each mode, the relative error is evaluated to have an estimate of the accuracy of the numerical method (*Table 4-4*).

<b>Mode</b>	<b>Anslys frequency [HZ]</b>	<b>Lusas frequency [HZ]</b>	<b>Analytic frequency [HZ]</b>	<b>%err respect Lusas</b>	<b>%err respect analytic</b>
<b>1<sup>st</sup> AS</b>	0.09464	0.09	0.0979	4.8	0.3
<b>1<sup>st</sup> S</b>	0.1323	0.128	0.1326	3.5	0.2
<b>2<sup>nd</sup>AS</b>	0.1937	0.186	0.1958	4.1	1
<b>2<sup>nd</sup> S</b>	0.1793	0.188	0.1875	4.8	4.5
<b>3<sup>rd</sup> AS</b>	0.2918	0.280	0.2936	4.2	0.6
<b>3<sup>rd</sup> S</b>	0.2459	0.238	0.2492	3.3	1.3

*Table 4-4: Results comparison and relative errors*

In *Table 4-4*, it is possible to observe how the differences in term of oscillation frequencies are very small, with a maximum relative error smaller than 4.8% respect to *Lusas* results and 4.5% respect to analytic ones.

### **4.3 Real case numerical example: *Singapore Suspension Footbridge***

It is possible to consider a numerical example realised with *ANSYS* program of a suspension footbridge of small span: the *Singapore Suspension Footbridge* (*Figure 4-15*). A plane model of the structure is realised and a modal analysis is performed with the goal of evaluating the natural frequencies to be compared to the ones obtained in the other methods, as in the previous cases analysed.

The structure examined is a footbridge realised in Singapore with a suspension span of 35 m (*Table 4-5*). It is designed respect to static actions and dynamic actions, as wind loads.

<b>Span</b>	35 m
<b>Width</b>	1.6 m
<b>Deck cross section</b>	$2.662 \cdot 10^{-2} \text{ m}^2$
<b>Deck density</b>	209 kg/m
<b><math>E_{\text{deck}}</math></b>	200 GPa
<b><math>I_{\text{deck}}</math></b>	$1.666 \cdot 10^{-4} \text{ m}^4$

<b><math>E_{\text{hangers}}</math></b>	100 GPa
<b><math>A_{\text{hangers}}</math></b>	$2.01 \cdot 10^{-4} \text{ m}^2$
<b><math>E_{\text{cable}}</math></b>	51.9 Gpa
<b><math>A_{\text{cable}}</math></b>	$3.504 \cdot 10^{-4} \text{ m}^2$
<b>Cable density</b>	5.569 kg/m
<b>Cable max displacement</b>	5.5 m
<b>Towers height</b>	6 m

Table 4-5: Mechanical and geometrical properties of Singapore Suspension Footbridge

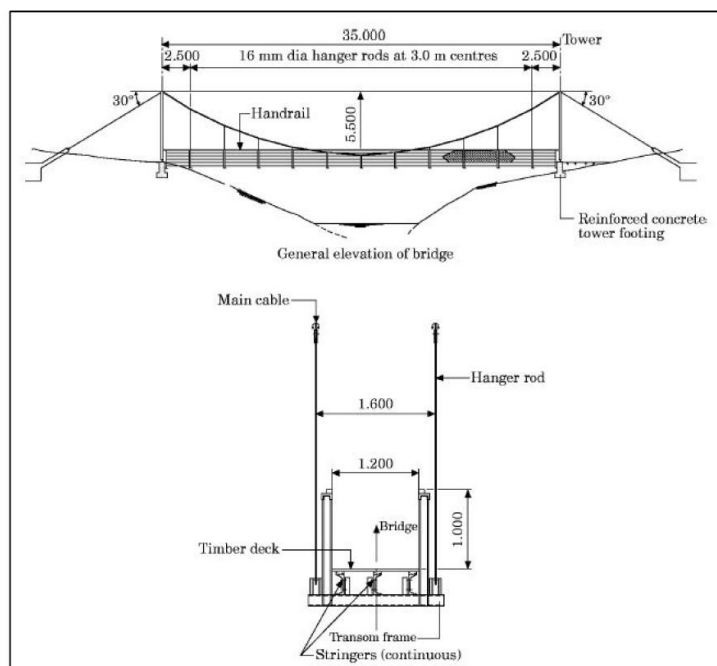


Figure 4-15: Geometrical properties of Singapore Suspension Footbridge

Main cable and deck are modelled in ANSYS using the element BEAM188 as in the previous cases. The hangers, that are subjected to axial forces to transmit loads from deck to main cable, are modelled using element LINK180 and their weight it is considered negligible.

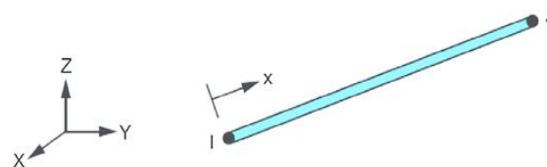


Figure 4-16: LINK180 representation[11]

LINK180 is a 3D element that can be used to model trusses, cables and links. It is a uniaxial tension-compression element with three degrees of freedom each node: translation in the nodal x, y and z directions. By default, this element includes stress-stiffness terms in any analysis that includes large-deflection effects. LINK180 is defined by two nodes, cross-sectional area and material properties, assigned in modelling phase. The mesh realised consists in a discretization of 200 elements for main cable and deck and each hanger is modelled as a single element. The static scheme considers hinges at the extremities of the main cable, whereas the deck is simply supported in vertical plane  $xy$ .

The results of modal analysis are shown in *Figure 4-17;4-19*:

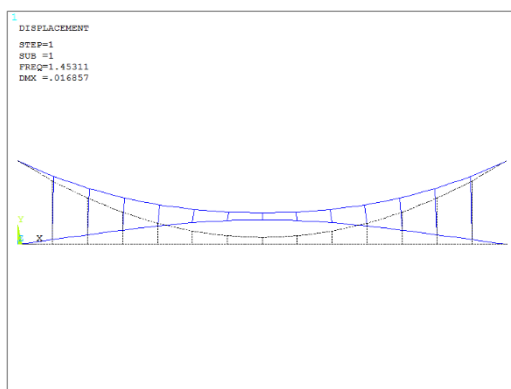


Figure 4-17: Mode 1 symmetric, 1.4531 Hz

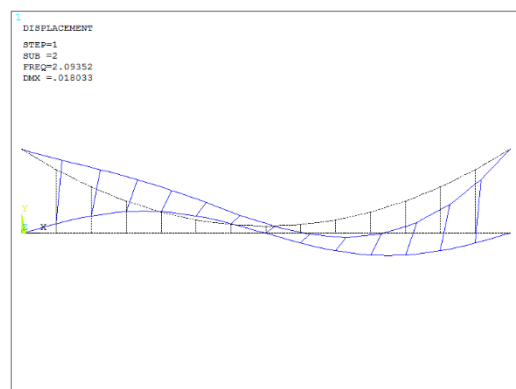


Figure 4-18: Mode 1 anti-symmetric, 2.0935 Hz

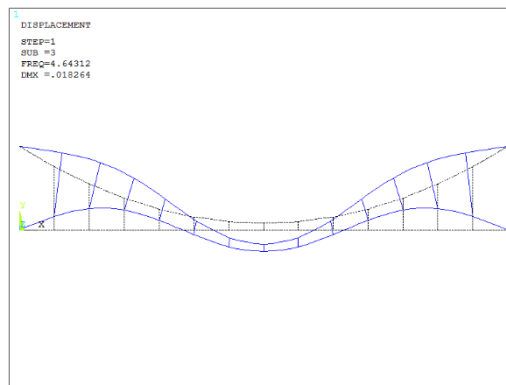


Figure 4-19: Mode 2 symmetric, 4.6431 Hz

The results obtained are compared with those obtained by analytic method (Lacarbonara, 2013[12]) and in *Lusas* (Table 4-6).

For the first symmetric mode, it is possible to observe a large difference between the results obtained by different methods, while for the other modes the relative errors decrease and values of natural frequencies converge.

<b>Mode</b>	<b>Ansys frequency [HZ]</b>	<b>Lusas frequency [HZ]</b>	<b>Analytic frequency [HZ]</b>	<b>%err respect Lusas</b>	<b>%err respect analytic</b>
<b>1<sup>st</sup> S</b>	1.4531	1.970	1.911	35.5	33.6
<b>1<sup>st</sup> AS</b>	2.0935	2.074	2.143	0.9	2.3
<b>2<sup>nd</sup> S</b>	4.6431	4.567	4.668	1.6	0.5

*Table 4-6: Results with different methods and relative errors*

## 4.4 Salvatori-Borri ideal bridge

A further development of the analysis realised in the previous *Chapters* allows to study a 3D model of a suspension bridge. In this way, its out of plane behaviour can be analysed, accounting for modal shapes and natural frequencies in horizontal direction and torsion.

The ideal model analysed by Salvatori-Borri in *Chap. 3.1* is studied, by realising a numerical model in ANSYS with the geometrical properties described in *Table 3-1*.

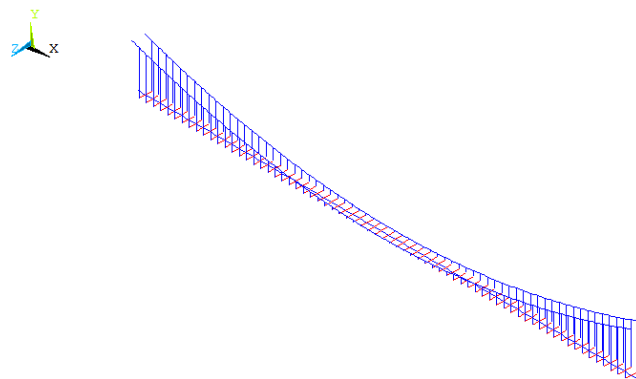


*Figure 4-20: "Fish-bone" ANSYS numerical model*

The "fish-bone" numerical model (*Figure 4-20*), is realised with ANSYS elements that allow considering geometric non-linearity when the analysis is developed.

In fact, the main cables are modelled using BEAM188 elements and they are restrained with hinges at the ends. The hangers, as in the case of plane model, are realised using element LINK180 that transmits only axial forces and their weight is negligible. The deck is modelled by element BEAM188 and it is connected to hangers by rigid links, that are fictitious elements

of the numerical model necessary to realise the connection. They are BEAM188 elements for which a very big inertia is assigned, to obtain a rigid flexural behaviour; their weight is imposed equal to zero. The static scheme of the deck provides a self-supported configuration in horizontal and vertical plane that permits rotations around  $y$  and  $z$  axes.

After the realisation of ANSYS numerical model, a modal analysis is performed as described in the previous cases and the following results are obtained (*Figure 4-21;4-26*):

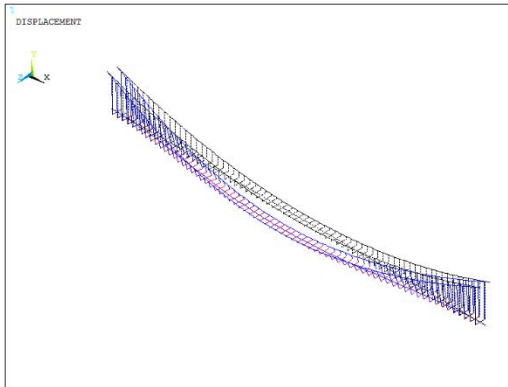


Figure 4-21: Mode 1 H-S, 0.08456 Hz

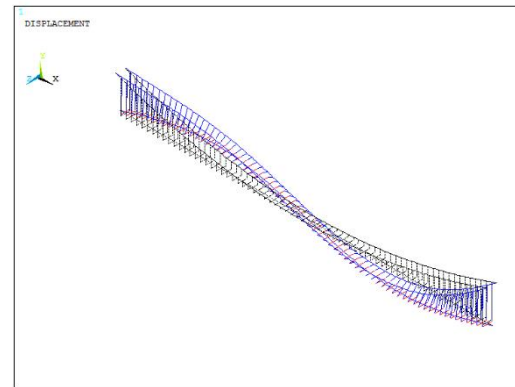


Figure 4-22: Mode 1 V-A, 0.1052 Hz

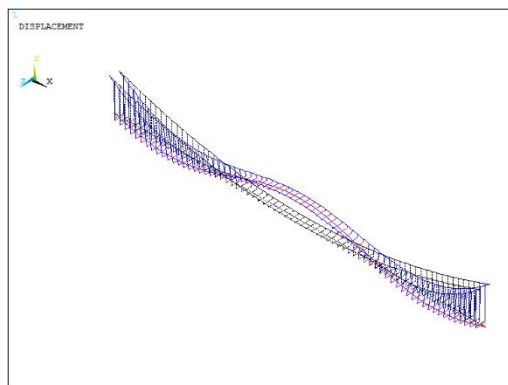


Figure 4-23: Mode 1 V-S, 0.1426 Hz

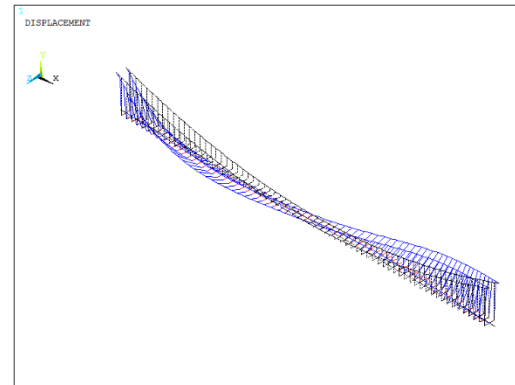


Figure 4-24: Mode 1 H-A, 0.1762 Hz

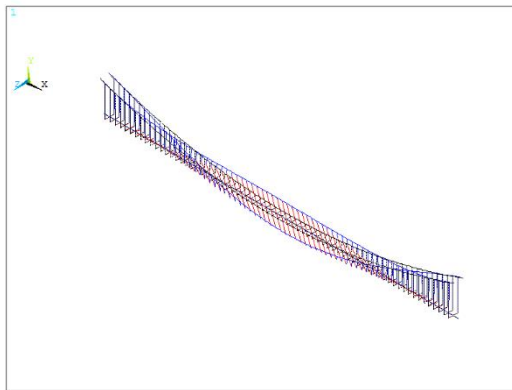


Figure 4-25: Mode 1 T-S, 0.3432 Hz

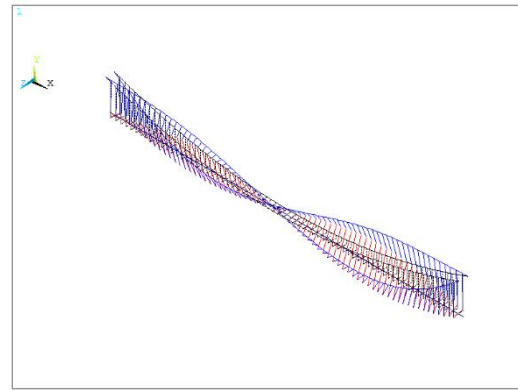


Figure 4-26: Mode 1 T-A, 0.3457 Hz

Mode	Frequency [Hz]
<b>1<sup>st</sup> H-S</b>	0.08456
<b>1<sup>st</sup> V-A</b>	0.1052
<b>1<sup>st</sup> V-S</b>	0.1426
<b>1<sup>st</sup> H-A</b>	0.1762
<b>2<sup>nd</sup> V-A</b>	0.2057
<b>2<sup>nd</sup> H-S</b>	0.2107
<b>2<sup>nd</sup> V-S</b>	0.2396
<b>2<sup>nd</sup> H-A</b>	0.2749
<b>3<sup>rd</sup> V-S</b>	0.2807
<b>3<sup>rd</sup> V-A</b>	0.3259
<b>3<sup>rd</sup> H-A</b>	0.3365
<b>1<sup>st</sup> T-S</b>	0.3432
<b>1<sup>st</sup> T-A</b>	0.3457

Table 4-7: Natural frequencies of Salvatori-Borri bridge

# CHAPTER 5

## AKASHI KAIKYO BRIDGE ANALYSIS

The finite elements numerical modelling of large suspension bridges is not an easy task, in fact, as showed in *Chap. 4*, these structures present a non-linear geometric behaviour, due to hangers and main cables. The increasing of load in hangers and cables, produced by the self-load of the bridge, causes an important stiffening effect on the structure.

The increasing of pull stress  $H$  in main cables generates a reduction of displacements given by further loads.

In suspension bridges, self-weight increases structural stiffness and it allows to support loads given by traffic or wind. These kinds of structures represent the easiest way to overcome big spans because, in unloaded condition, the elements that support permanent load are hangers and cable, whereas the deck is free by stresses.

So, it is necessary to use a software that can take into account specific effects and that allows to solve an eigenvalues problem. The software must also consider unsteady forces acting on the bridge, to perform a flutter analysis.

The structure analysed in this chapter is the *Akashi Kaikyo Bridge* that, with its 1991 m of main span, is today the longest suspension bridge in the world.

Two different numerical models of the bridge were realised: the first is a “Fish-bone” model, where after the definition of natural frequencies, a first flutter analysis is performed. The second is a more realistic model with a complex truss deck, that allows to consider with more accuracy the torsional behaviour of the suspension bridge and performs a more efficient flutter analysis.

The construction of the *Akashi Kaikyo Bridge* ended in 1998 and links the city of Kobe on the Japanese mainland of Honshu to Iwaya on Awaji Island. It crosses the busy Akashi Strait as part of the Honshu–Shikoku Highway. Its main cable, with a total diameter of 1.6 m present a new technology of maintenance the “*Dry air injection system*” to

protect from corrosion. The system consists in injecting dry air into main cables and to keep the humidity inside the cables at a constant value. This system is a revolutionary idea because in this way the maintenance cost can be highly reduced.

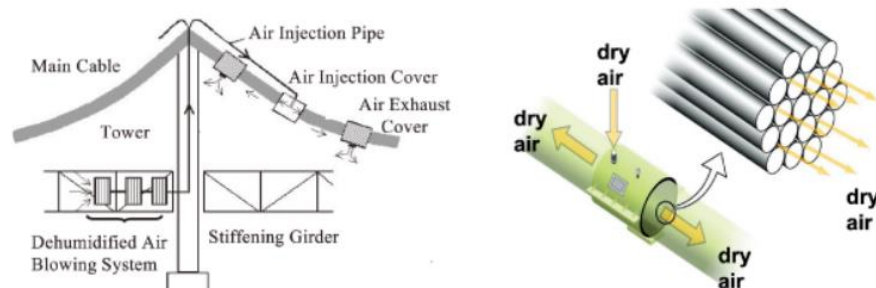


*Figure 5-1: Dry air injection system*

For the construction of deck beams (*Figure 5-2*) 90,000 tons of reinforcement steel have been used. Due to the large size of the bridge, the wind load which must face is higher than that of any other existing bridge at the completion of construction. Using steel with high tensile strength for the beams made very strong yet lightweight, and thus cheaper. The reinforcing elements are prefabricated shaped panel and transported to the construction site where they have been erected into the interior of the anchorages and towers with floating cranes.



*Figure 5-2: View of Akashi Kaikyo Bridge*

## 5.1 “Fish-bone” model

The ANSYS numerical model is realised with the geometrical properties shown in *Table 3-2*. A “Fish-bone” model (*Figure 5-3*) of the central span was realised. For the main

cables a reduced elastic modulus  $E^* = 1.6 \cdot 10^{10} Pa$  was used, taking into account the deformability of the side cables over the lateral spans of 960.

The main cables are modelled using BEAM188 elements, as in Salvatori-Borri case, and they are restrained with hinges at the extremities. The hangers are realised using element LINK180 that transmits only axial forces and their weight is negligible. The deck is modelled with element BEAM188 and it is connected to hangers by rigid links, fictitious elements of the numerical model necessary to realise the connection. They are BEAM188 elements for which a very big inertia is assigned to obtain rigid flexural behaviour and their weight is imposed equal to zero. The static scheme of the deck provides a self-supported configuration in horizontal and vertical plane that allows rotations around  $y$  and  $z$  axes (*Figure 5-3*).

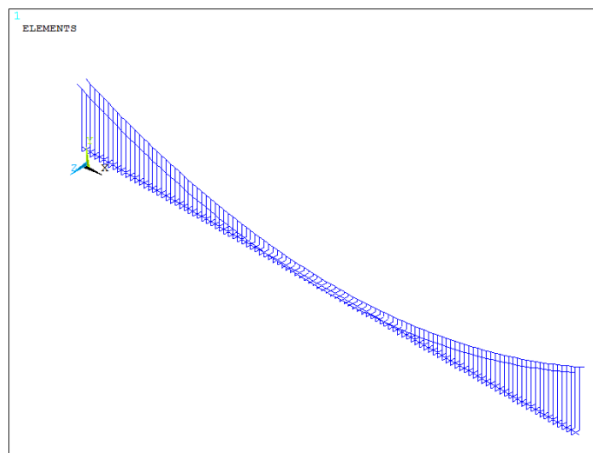


*Figure 5-3: Akashi Kaikyo "Fish-bone" numerical model*

After the realisation of ANSYS numerical model, a modal analysis was performed as described in previous cases and the following results were obtained (*Figure 5-4;5-9*):

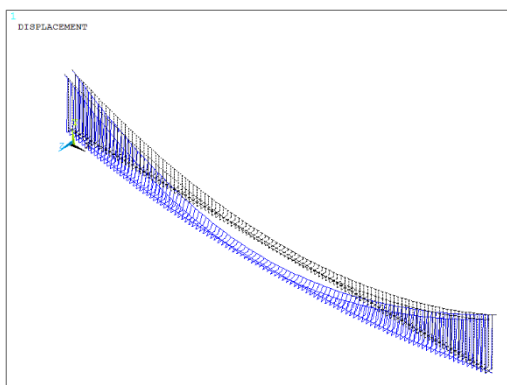


*Figure 5-4: Mode 1 H-S, 0.0366 Hz*

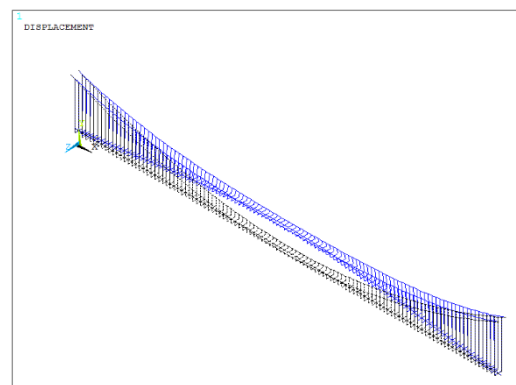


*Figure 5-5: Mode 1 V-S, 0.0593 Hz*

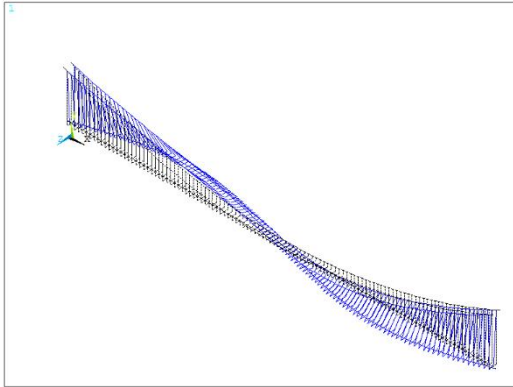


Figure 5-6: Mode 1 H-A, 0.0654 Hz

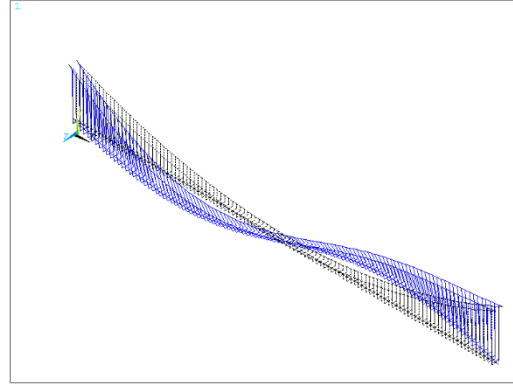


Figure 5-7: Mode 1 V-A, 0.0815 Hz

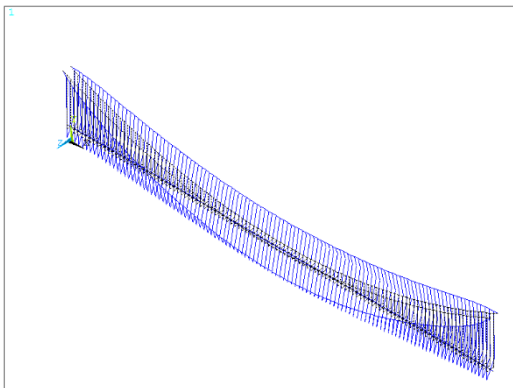


Figure 5-8: Mode 1 T-S, 0.132 Hz

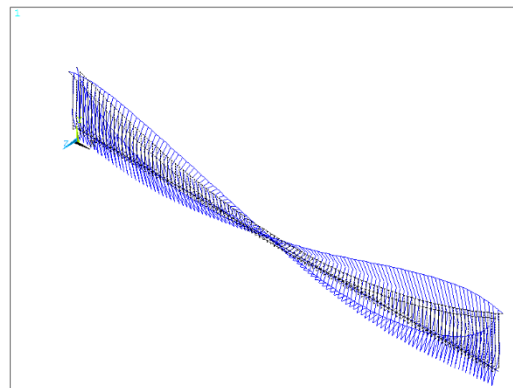


Figure 5-9: Mode 1 T-A, 0.203 Hz

ANSYS modal analysis results are compared to those obtained by D'Argenio by a continuous model (*Chap 3.2.2*) and results from the literature (*Bridge Aeroelasticity, Chap. 3.2.1*). The relative errors between the three different methods in terms of frequency are shown in *Table 5-1*.

Mode	ANSYS results [Hz]	Analytic results [Hz]	Literature results [Hz]	%err respect analytic	%err respect literature
1 <sup>st</sup> H-S	0.0366	0.027	0.045	35	22
1 <sup>st</sup> V-S	0.0593	0.066	0.065	11	10
1 <sup>st</sup> H-A	0.0653	0.075	0.084	15	28
1 <sup>st</sup> V-A	0.0815	0.077	0.085	5.8	4.3
2 <sup>nd</sup> V-S	0.118	0.120	0.122	1.7	3.4

<b>1<sup>st</sup> T-S</b>	0.132	0.124	0.129	6.4	2.3
<b>2<sup>nd</sup> V-A</b>	0.159	0.164	0.171	3.1	7.5
<b>1<sup>st</sup> T-A</b>	0.203	0.212	0.210	4.4	3.4

*Table 5-1: Akashi Kaikyo Bridge modal analysis results*

The relative errors are not negligible for lower frequencies, while they become smaller for the higher modes.

### 5.1.1 Flutter analysis

After the evaluation of natural vibration frequencies, it is possible to perform a flutter analysis of the *Akashi Kaikyo Bridge*. The aim of flutter analysis is to predict the lowest critical wind velocity that induces flutter instability, and the corresponding flutter frequency.

The procedure adopted to perform the analysis in *ANSYS* software is described in the article by *X.G. Hua et al., 2007* [13].

The numerical model uses a specific element, *MATRIX27*, in *ANSYS* to model the aeroelastic forces acting on the bridge, where the stiffness and damping matrices are expressed in terms of the reduced wind velocity and flutter derivatives. With the use of this FE model, damped complex eigenvalue analysis is carried out to determine the complex eigenvalues, of which the real part is the logarithm decay rate and the imaginary part is the damped vibration frequency. The condition for onset of flutter instability becomes that, at a certain wind velocity, the structural system incorporating fictitious *MATRIX27* elements has a complex eigenvalue with zero or near-zero real part, with the imaginary part of this eigenvalue being the flutter frequency.

The equation of motion of a bridge structure in the smooth flow can be expressed as:

$$[M]\{\ddot{X}\} + [C]\{\dot{X}\} + [K]\{X\} = \{F_{se}\} \quad (5-1)$$

where:

- $M, C, K$ : are the global mass, damping and stiffness matrices;
- $\ddot{X}, \dot{X}, X$ : represent nodal acceleration, velocity and displacement vectors;
- $F_{se}$ : is the vector of nodal aeroelastic forces.

The aeroelastic forces (Figure 5-10) acting on unit span of bridge girder can be expressed as a linear function of nodal displacement and velocity (Scanlan 1978):

$$L_{se} = \frac{1}{2} \rho U^2 (2B) \left[ KH_1^* \frac{\dot{h}}{U} + KH_2^* \frac{B\dot{\alpha}}{U} + K^2 H_3^* \alpha + K^2 H_4^* \frac{h}{B} + KH_5^* \frac{\dot{p}}{U} + K^2 H_6^* \frac{p}{B} \right] \quad (5-2)$$

$$D_{se} = \frac{1}{2} \rho U^2 (2B) \left[ KP_1^* \frac{\dot{p}}{U} + KP_2^* \frac{B\dot{\alpha}}{U} + K^2 P_3^* \alpha + K^2 P_4^* \frac{p}{B} + KP_5^* \frac{\dot{h}}{U} + K^2 P_6^* \frac{h}{B} \right] \quad (5-3)$$

$$M_{se} = \frac{1}{2} \rho U^2 (2B^2) \left[ KA_1^* \frac{\dot{h}}{U} + KA_2^* \frac{B\dot{\alpha}}{U} + K^2 A_3^* \alpha + K^2 A_4^* \frac{h}{B} + KA_5^* \frac{\dot{p}}{U} + K^2 A_6^* \frac{p}{B} \right] \quad (5-4)$$

where:

- $\rho$ : is the air mass density, 1.27 [kg/m<sup>3</sup>];
- $U$ : is the wind speed;
- $B$ : is the width of bridge deck;
- $K = \frac{\omega B}{U}$ : is the reduced circular frequency;
- $h, p, \alpha$ : are the vertical, lateral and torsional displacement, respectively;
- $A_i^*, H_i^*, P_i^*$ : are non-dimensional flutter derivatives, which are function of reduced wind speed and they are evaluated in wind tunnel.

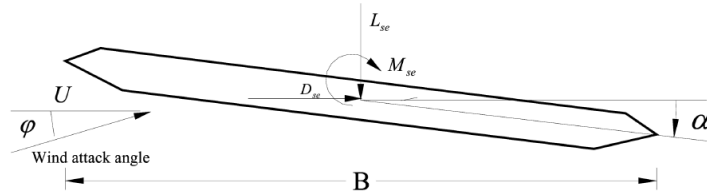


Figure 5-10: Deck section representation

In finite element analysis, these distributed forces are converted into equivalent nodal loadings acting at the member ends. Thus, aeroelastic forces for element  $e$  can be expressed in terms of nodal displacement and nodal velocity as:

$$\{F_{ae}\} = [C]_{ae}^e \{\dot{X}\}^e + [K]_{ae}^e \{X\}^e \quad (5-5)$$

Where  $[K]_{ae}^e, [C]_{ae}^e$  represent the local aeroelastic stiffness and damping matrices for element  $e$ , respectively.

Using the lumped formulation, the expressions of  $[K]_{ae}^e, [C]_{ae}^e$  are obtained as:

$$[K]_{ae}^e = \begin{bmatrix} K_{ae1}^e & 0 \\ 0 & K_{ae1}^e \end{bmatrix} \quad (5-6)$$

$$[C]_{ae}^e = \begin{bmatrix} C_{ae1}^e & 0 \\ 0 & C_{ae1}^e \end{bmatrix} \quad (5-7)$$

$$[K]_{ae1}^e = a \begin{bmatrix} 0 & 0 & 0 & 0 & 0 & 0 \\ 0 & P_6^* & P_4^* & BP_3^* & 0 & 0 \\ 0 & H_6^* & H_4^* & BH_3^* & 0 & 0 \\ 0 & BA_6^* & BA_4^* & B^2A_3^* & 0 & 0 \\ 0 & 0 & 0 & 0 & 0 & 0 \\ 0 & 0 & 0 & 0 & 0 & 0 \end{bmatrix} \quad (5-8)$$

$$[C]_{ae1}^e = b \begin{bmatrix} 0 & 0 & 0 & 0 & 0 & 0 \\ 0 & P_5^* & P_1^* & BP_2^* & 0 & 0 \\ 0 & H_5^* & H_1^* & BH_2^* & 0 & 0 \\ 0 & BA_5^* & BA_1^* & B^2A_2^* & 0 & 0 \\ 0 & 0 & 0 & 0 & 0 & 0 \\ 0 & 0 & 0 & 0 & 0 & 0 \end{bmatrix} \quad (5-9)$$

where:

- $a = \frac{1}{2} \rho U^2 K^2 L_e$ ;
- $b = \frac{1}{2} \rho U K L_e$ ;
- $L_e$ : is the length of fictitious element.

The user-defined element in ANSYS, MATRIX27, is an element with two nodes with six degrees of freedom each one (Figure 5-11), and with its local coordinate system being coincident with the global coordinate system. The element is arbitrary in geometrical configuration and the element properties are specified by stiffness, mass, and damping coefficients.

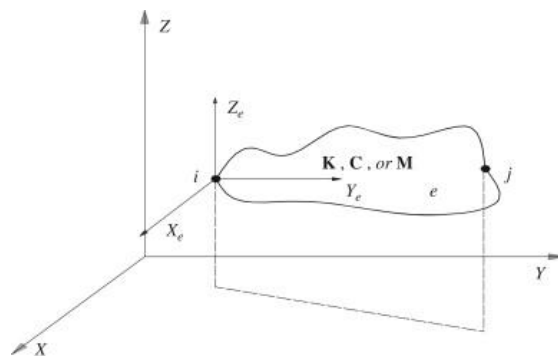


Figure 5-11: Matrix27 ANSYS element[14]

The first step for flutter analysis using ANSYS is to simulate the aeroelastic forces acting on each node by element MATRIX27. To achieve this, a hybrid FE model incorporating one structural element with four MATRIX27 elements as illustrated in *Figure 5-12* is formulated. Considering the fact that one MATRIX27 element can only model either an aeroelastic stiffness matrix or an aeroelastic damping matrix instead of both simultaneously, a pair of MATRIX27 elements are attached every node in a structural element to simulate the aeroelastic forces. For a deck element  $e$  as shown in *Figure 5-12*, MATRIX27 elements  $e1$  and  $e3$  are attached after defining a fictitious node  $k$  to represent the aeroelastic stiffness and damping at node  $i$ , while MATRIX27 elements  $e2$  and  $e4$  are attached after defining a fictitious node  $l$  to represent the aeroelastic stiffness and damping at node  $j$ . The pair of MATRIX27 elements attached to each structural node share the same nodes.



*Figure 5-12: Hybrid finite element model for flutter analysis in ANSYS*

Now it is possible to assemble all element matrices into global aeroelastic stiffness and damping matrices:

$$[F]_{ae} = [K]_{ae}\{X\} + [C]_{ae}\{\dot{X}\} \quad (5-10)$$

Substituting *Eq. 5-10* in *Eq. 5-1* results in the governing equation of motion for the structure after incorporating MATRIX27 elements, as:

$$[M]\{\ddot{X}\} + ([C] - [C]_{ae})\{\dot{X}\} + ([K] - [K]_{ae})\{X\} = 0 \quad (5-11)$$

With this equation, damped complex eigenvalue analysis can be carried out to determine the characteristic of the parametrized system. The dynamic response can be approximated by a superposition of the first  $m$  conjugate pairs of complex eigenvalues and eigenvectors, as:

$$X = \sum_{j=1}^m \phi_j e_j^{\lambda_j t} \quad (5-12)$$

where:

- $\phi_j = p_j \pm iq_j$ : is the  $j^{\text{th}}$  complex conjugate pair of eigenvectors;
- $\lambda_j = \sigma_j \pm i\omega_j$ .

The system is dynamically stable if the real part of all eigenvalues is negative and dynamically unstable if the real part of one or more eigenvalues is positive. The condition for

occurrence of flutter instability is then identified as follows: for certain wind velocity  $U_f$  the system has one complex eigenvalue  $\lambda_f$  with zero or near zero real part, the corresponding wind velocity  $U_f$  being the critical flutter wind velocity and the imaginary part of the complex eigenvalue  $\lambda_f$  becoming the flutter frequency.

MATRIX27 elements were incorporated in the numerical model of *Akashi Kaikyo Bridge* to perform flutter analysis for a real case. Two hybrid elements ( $L_e$  unitary value), for aeroelastic stiffness and damping, respectively, have been attached at each node and they are fully restrained at their extremities (*Figure 5-13*).

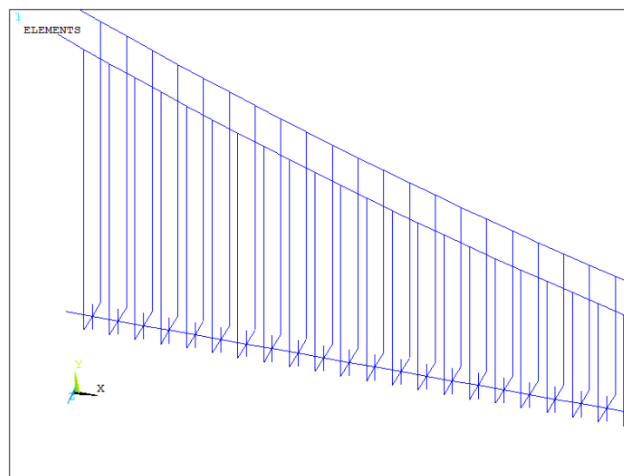


Figure 5-13: Hybrid ANSYS model of Akashi Kaikyo Bridge, with MATRIX27 elements

Because of the impossibility to know the complex mode which corresponds to a real flutter frequency a priori, a mode-by-mode tracing method is employed to iteratively search the flutter frequency and determine the critical flutter wind velocity. The procedure in ANSYS is summarized in the following steps:

1. Establish the initial structural FE model without MATRIX27 elements and compute the first  $m$  natural modes  $\omega_i^0 (i=1, \dots, m)$ ;
2. Establish the FE model of the integrated system with MATRIX27 elements, in which the flutter derivatives are inputted through the command *TABLE* in ANSYS;
3. Set an initial guess of critical wind velocity  $U_0$  and its increment  $\Delta U$ . Let the initial oscillation frequency  $\omega_0$  be the frequency  $\omega_i^0$  of each natural mode in turn. Given the tolerance  $\epsilon$ ;
4. Determine the reduced wind velocity and the aeroelastic stiffness and damping matrices in MATRIX27 elements at the present iteration, and then carry out the damped eigenvalue analysis;

5. Compare the imaginary part of the  $i^{\text{th}}$  computed complex eigenvalue  $\lambda_i$  with  $\omega_0$ . If  $\left| \frac{Im(\lambda_i) - \omega_0}{Im(\lambda_i)} \right| > \epsilon$ , let  $\omega_0 = Im(\lambda_i)$  and repeat steps 4 and 5, otherwise go to step 6;
6. Repeat steps 4 and 5 over all  $m$  computed natural modes. If the real parts of all complex eigenvalues  $\lambda_i (i=1, \dots, m)$  are negative, let  $U = U_0 + \Delta U$  and repeat steps 4 and 5, otherwise when real part for one mode become equal to zero, it is obtained flutter critic speed.

To assemble the MATRIX27 for each wind speed, flutter derivates, function of reduced wind speed in terms of  $A_i$ ,  $P_i$ ,  $H_i$  (Figure 5-14), are necessary to obtain the formulations of the three unsteady forces acting on the deck:  $L_{ns}$ ,  $D_{ns}$ ,  $M_{ns}$ .

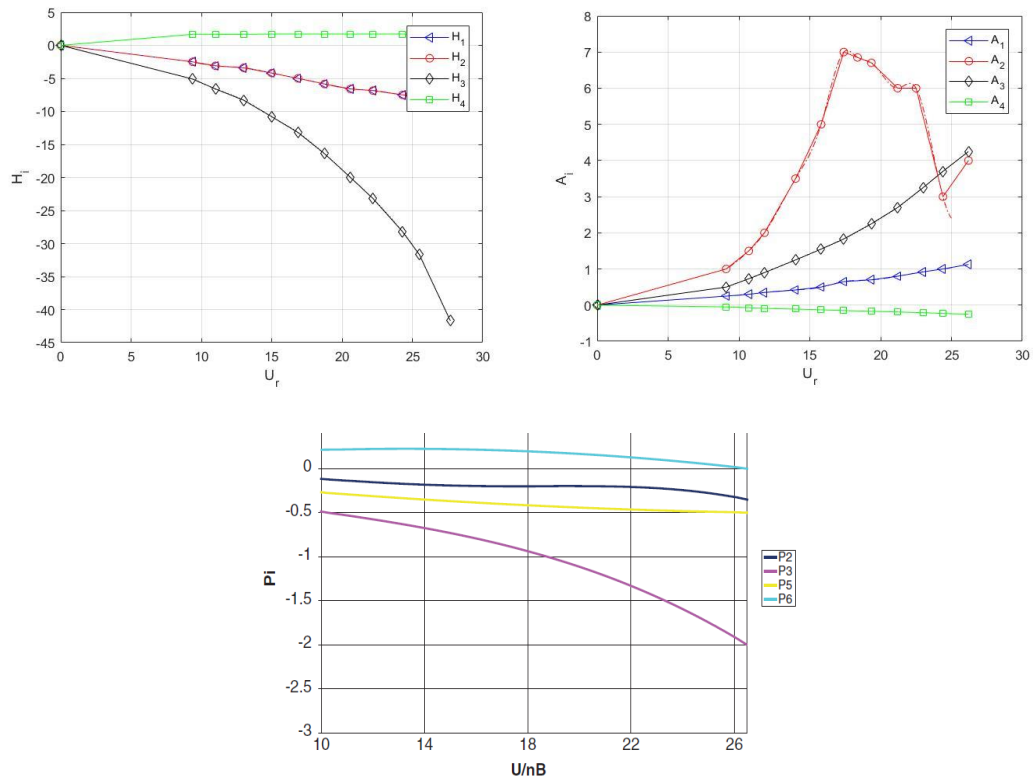


Figure 5-14: Flutter derivates for Akashi Kaikyo Bridge

## Analysis results

The above-described method is used to perform a flutter analysis on the *Akashi Kaikyo Bridge*, with “Fish-bone” numerical model. Using that structural approximation, the model is not able to analyse the torsional behaviour of the bridge under wind effects. In fact, the iterative method does not evaluate correctly torsional frequencies and their modal shapes,

changing wind speed. The eigenvalue relative at the first symmetric vertical mode is the only one that is obtained in the damped modal analysis, and its real and imaginary part are correctly evaluated, for each wind speed.

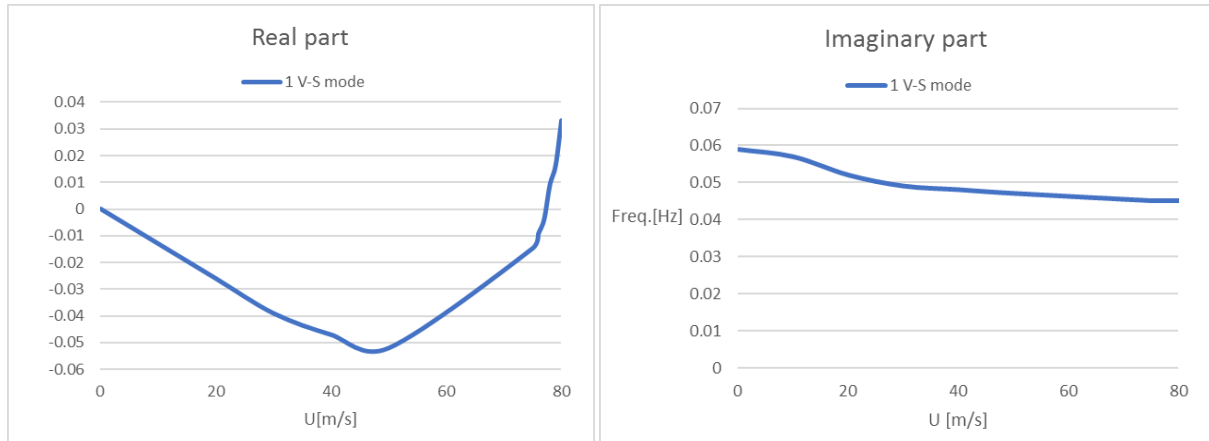


Figure 5-15: Real part eigenvalue (left), imaginary part (right)

The iterative procedure starts from an initial wind speed of  $U_0 = 0$  m/s, and the increasing of wind speed  $\Delta U$  in the procedure has been fixed to 10 m/s for each analysis, till a design value of arrive to  $U = 70$  m/s. After this point, the discretization step-by-step of  $\Delta U$  was set to  $\Delta U = 1$  m/s, because the real part of the eigenvalue is approaching zero. The analysis furnished a flutter critic speed  $U_f = 77.2$  m/s, given by 1<sup>st</sup> V-S mode with a frequency of 0.045 Hz (Figure 5-15). The results are compared to that reported in the literature (“Bridge aeroelasticity”[6] obtained as average value between analytic, numerical and reduced model methods, “Aeroelastic Phenomena”[15] obtained with numerical model) and with that obtained by Maldera by *MATLAB* program (Table 5-2).

	<b>ANSYS results</b>	<b>Literature data</b>	<b>Analytic results</b>	<b>%err literature</b>	<b>%err analytic</b>
<b><math>U_{cr}</math> [m/s]</b>	77.2	77.7	75.6	0.6	2.1
<b><math>f_{cr}</math> [Hz]</b>	0.045	0.138	0.075	206	83

Table 5-2: Akashi Kaikyo Bridge flutter analysis results comparison

Observing Table 5-2, it is clear how the flutter critic speed, obtained in ANSYS with “Fish-bone” model, shows a very small relative error respect to literature data and analytic model. Much bigger differences can be evaluated considering flutter critical frequency with a relative error bigger than 200% between ANSYS results and bibliographic data. But, the more considerable difference is that the results showed in literature and those obtained with analytic

methods display first torsional symmetric mode as responsible of flutter instability. Whereas, the numerical model, realised in ANSYS, showed that the flutter instability is associated to the first symmetric vertical mode. So, it is possible to assert that the “Fish-bone” numerical model of *Akashi Kaikyo Bridge* produces good results in terms of flutter critical wind speed, but it does not show the correct mode responsible of the phenomenon.

## 5.2 “Truss-beam” deck model

The “Fish-bone” model of the *Akashi Kaikyo Bridge*, analysed in *Chap 5.1*, shows good results in terms of natural frequencies and mode-shapes compared to literature data. In the flutter analysis, considering the mode-shape responsible of the phenomenon, it is possible to evaluate a difference respect the results of analytic analysis and bibliographic data that show first torsional symmetric mode as the responsible of the instability.

For this reason, it is possible to improve the numerical model analysed, with the realisation of a truss beam deck model that represents, with a better accuracy, the real structure of the *Akashi Kaikyo Bridge*. The aim of this model is to analyse correctly the torsional behaviour of the deck under wind action and to obtain a better solution in term of critical wind speed, frequency and mode-shape that cause flutter instability.

The structure is modelled with four main longitudinal beams connected by transversal elements and two secondary longitudinal beams in the bottom part of the deck. There are stiffeners in longitudinal direction that transmits load between top and bottom longitudinal beam, and transversal elements orthogonal respect the axis of the deck. In the bottom part of the deck, V-shaped elements are assembled with the up-wind function (*Figure 5-16*). The numerical model is realised with the assembly in the longitudinal direction of the same module 40 m long.

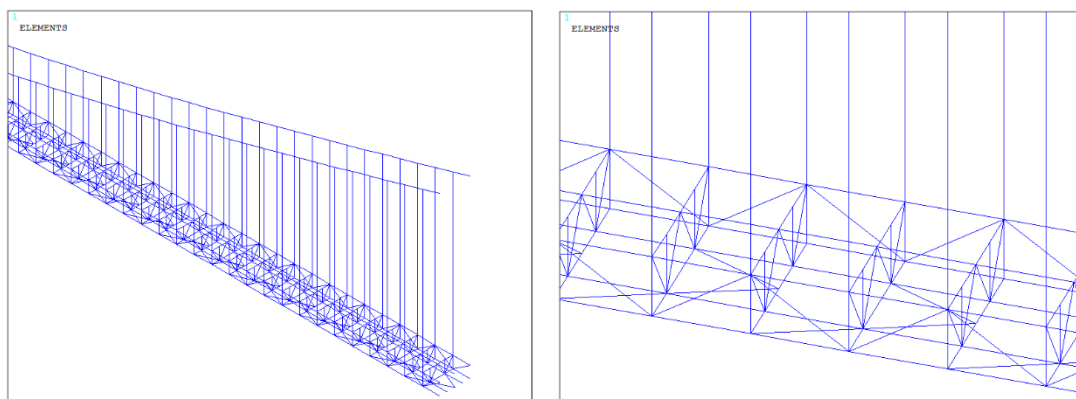


Figure 5-16: “Truss-beam” deck ANSYS numerical model



*Figure 5-17: Akashi Kaikyo Bridge rendering model*

Material properties are the same of the “Fish-bone” model showed in *Table 3-2*. The numerical model in *ANSYS* is realised using *BEAM188* elements for main cables and deck elements, whereas *LINK180* element is assigned to hangers. The static scheme considers hinges at the extremity of main cables and the deck is restrained as simply supported beam in vertical plane *xy*, whereas, due to huge stiffness in horizontal plane *xz*, it is fully restrained in the other directions. The geometrical properties of “truss-beam” deck are showed in following *Table 5-3*:

	<b>A [m<sup>2</sup>]</b>	<b>I<sub>xx</sub> [m<sup>4</sup>]</b>	<b>I<sub>yy</sub> [m<sup>4</sup>]</b>
<b>Longitudinal beams</b>	1.05	0.0757	0.111
<b>Longitudinal secondary beams</b>	0.410	0.0139	0.0139
<b>Longitudinal stiffeners</b>	0.533	0.0236	0.0236
<b>Transversal stiffeners</b>	0.372	0.0165	0.0080
<b>V-shaped up-winds</b>	0.358	0.0122	0.00936

*Table 5-3: Geometrical properties of “truss-beam” deck*

### 5.2.1 Modal analysis

After the realisation of *ANSYS* numerical model, a modal analysis was performed as described in the previous cases and natural frequencies and modal shapes of the “truss-beam” model are evaluated. *ANSYS* results are compared to those obtained by D’Argenio with analytic method (*Chap 3.2.2*) and the data reported in literature (*Bridge Aeroelasticity, Chap. 3.2.1*). They are evaluated the relative errors between the three different methods in term of frequency for each natural mode (*Table 5-4*).

<b>Mode</b>	<b>ANSYS results [Hz]</b>	<b>Analytic results [Hz]</b>	<b>Literature data [Hz]</b>	<b>%err respect analytic</b>	<b>%err respect literature</b>
<b>1<sup>st</sup> H-S</b>	0.0463	0.027	0.045	71	2.8
<b>1<sup>st</sup> V-S</b>	0.100	0.066	0.065	51	52
<b>1<sup>st</sup> H-A</b>	0.077	0.075	0.084	2.6	9
<b>1<sup>st</sup> V-A</b>	0.102	0.077	0.085	32.4	20
<b>2<sup>nd</sup> V-S</b>	0.158	0.120	0.122	31	29
<b>1<sup>st</sup> T-S</b>	0.142	0.124	0.129	14.5	10
<b>2<sup>nd</sup> V-A</b>	0.229	0.164	0.171	39.6	33.9
<b>1<sup>st</sup> T-A</b>	0.203	0.212	0.210	4.4	3.4

*Table 5-4: Modal analysis “truss-beam” model results*

It is possible to underline an increasing of relative errors respect the case of “Fish-bone” model, more considerable for vertical modes. In fact, the literature data and the analytic analysis are obtained modelling the deck as a simple beam, whereas in “truss beam” model there is an increasing of deck’s stiffness that generate different results respect the previous case.

## 5.2.2 Flutter analysis

After the modal analysis, a flutter analysis of the *Akashi Kaikyo Bridge* was performed. The procedure is the one adopted for the “Fish-bone” model.

The flutter analysis was performed by three approaches where the wind actions applied on the bridge (Drag, Lift and Moment) are modelled in different ways:

- Drag, Lift and Moment are modelled as three unsteady actions;
- Lift and Moment are modelled as unsteady actions and Drag is a steady horizontal force;
- Lift and Moment are unsteady actions, whereas Drag contribution is neglected.

## ***Lift, Drag and Moment unsteady analysis***

The analysis can be performed as shown in case of “Fish-Bone” model; Lift, Drag and Moment are expressed by Eq. 5-2;5-3;5-4 and they are applied as shown in Figure 5-18:

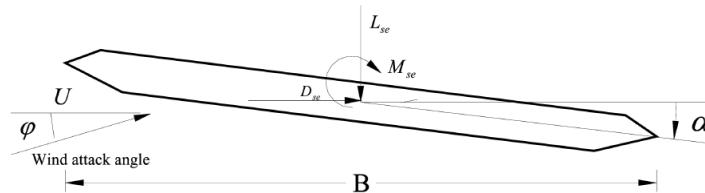


*Figure 5-18: Deck section and actions representation*

The hybrid numerical model uses the element MATRIX27 in ANSYS to model the aeroelastic forces acting on the bridge, in a way that the stiffness and damping matrices are expressed in terms of the reduced wind velocity and flutter derivatives. The fictitious elements MATRIX27 have a unitary length and they are realised with a constant interaxial distance and connected to the middle axis of the deck, as showed in Figure 5-13 for the “Fish-bone” model.

By the “truss-beam” modelling, damped complex eigenvalue analysis is correctly performed in terms of real and imaginary part also respect to torsional mode-shapes and so, there is an improvement of the solution respect to “Fish-bone” model, which, by contrast, is not able to evaluate torsional behaviour in the flutter instability. First torsional and vertical modes are analysed in the solution, in both symmetric and anti-symmetric configuration.

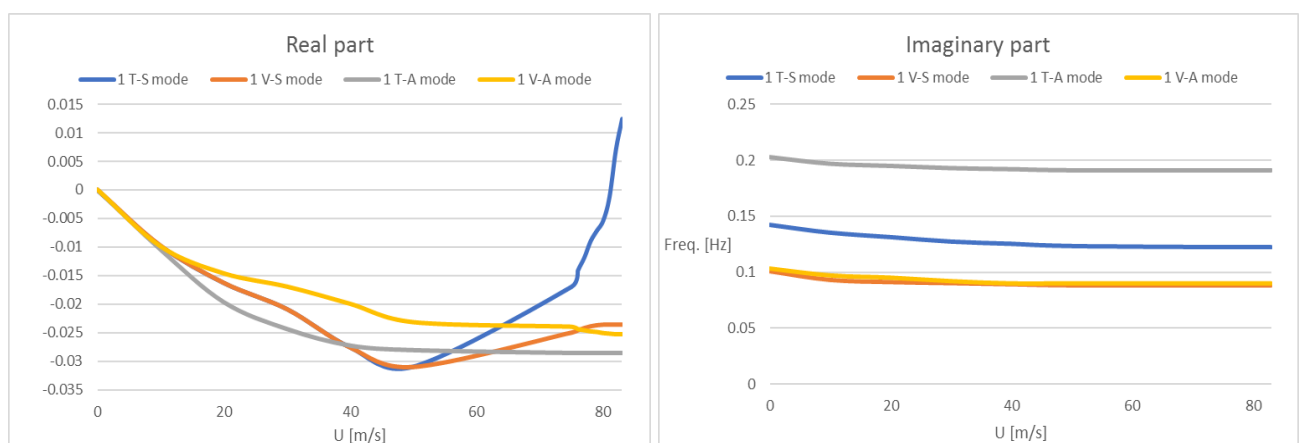


*Figure 5-19: Real (left) and imaginary (right) part of the solution*

The analysis evaluates a flutter critic speed  $U_f = 81.3$  m/s, given by 1<sup>st</sup> T-S mode, (Figure 5-19) with an horizontal component of displacement and a critical frequency of 0.122

Hz (Figure 5-20). It is possible to observe that damped modal analysis gives a small reduction of vibration frequencies for each natural mode, as wind speed is increased.

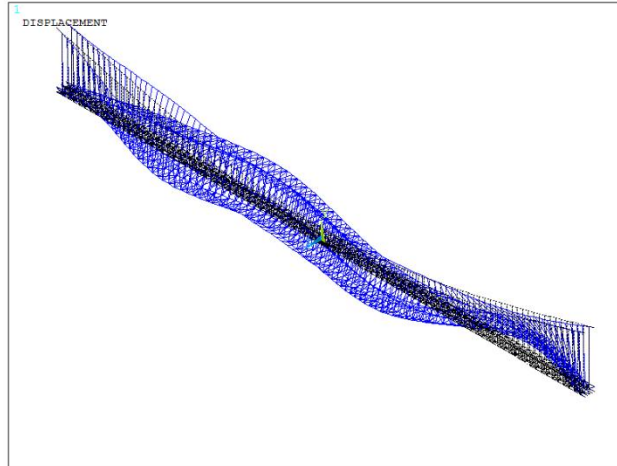


Figure 5-20: Critical flutter mode-shape

The results, as for “Fish-bone” model, are compared to those reported in the literature (“*Bridge aeroelasticity*”[6], “*Aeroelastic Phenomena*”[15]), and with those obtained by Maldera in *MATLAB* (Table 5-5).

	<b>ANSYS results</b>	<b>Literature data</b>	<b>Analytic results</b>	<b>%err literature</b>	<b>%err analytic</b>
<b><math>U_{cr}</math> [m/s]</b>	81.3	77.7	75.6	4.6	7.5
<b><math>f_{cr}</math> [Hz]</b>	0.122	0.138	0.075	13	62

Table 5-5: Akashi Kaikyo Bridge flutter analysis, with three *n-s* actions, results comparison

It is possible to observe that the flutter critic speed, obtained in ANSYS with “truss-beam” model, presents a relative error respect to literature data smaller than 5% and of 7.5% respect to analytic model. More important differences can be evaluated considering flutter critical frequency, with a relative error of 13% between ANSYS results and literature data. Respect to the case of “fish-bone” model, it is possible to observe a small increase in critical wind speed of about 5 m/s, that presents a relative error smaller than 1%, compared to bibliographic data for Akashi Kaikyo Bridge. “Truss-beam” analysis gives result with higher accuracy in terms of critical flutter frequency, but the most important improvement is the identification of the mode-shape associated to the instability that is, as in the literature data and analytic results, the first torsional symmetric mode.

### ***L-M unsteady, Drag steady actions***

As in the previous case, Lift and Moment are considered as unsteady actions and they are evaluated in function of flutter derivatives  $H_i, A_i$ . In addition, in this case the Drag horizontal action is modelled as a steady force acting on the deck and it is function of aerodynamic resistance factor  $C_d$  (Table 3-5):

$$D_s = \frac{1}{2} \rho U^2 B C_d(0) \quad (5-13)$$

Drag force is evaluated for each wind speed considered in the analysis, for an angle of attack  $\alpha = 0$ . The hybrid numerical model utilises the element MATRIX27 in ANSYS to model the aeroelastic forces acting on the bridge, in a way that the stiffness and damping matrices are expressed in terms of the reduced wind velocity and flutter derivatives. In this case, the terms in the matrices, depending on unsteady Drag, are set equal to zero.

$$[K]_{ae1}^e = a \begin{bmatrix} 0 & 0 & 0 & 0 & 0 & 0 \\ 0 & 0 & 0 & 0 & 0 & 0 \\ 0 & H_6^* & H_4^* & BH_3^* & 0 & 0 \\ 0 & BA_6^* & BA_4^* & B^2 A_3^* & 0 & 0 \\ 0 & 0 & 0 & 0 & 0 & 0 \\ 0 & 0 & 0 & 0 & 0 & 0 \end{bmatrix} \quad (5-14)$$

$$[C]_{ae1}^e = b \begin{bmatrix} 0 & 0 & 0 & 0 & 0 & 0 \\ 0 & 0 & 0 & 0 & 0 & 0 \\ 0 & H_5^* & H_1^* & BH_2^* & 0 & 0 \\ 0 & BA_5^* & BA_1^* & B^2 A_2^* & 0 & 0 \\ 0 & 0 & 0 & 0 & 0 & 0 \\ 0 & 0 & 0 & 0 & 0 & 0 \end{bmatrix} \quad (5-15)$$

where:

- $[K]_{ae}^e, [C]_{ae}^e$  represent the local aeroelastic stiffness and damping matrices for element  $e$ , respectively, without Drag terms;
- $a = \frac{1}{2} \rho U^2 K^2 L_e$ ;
- $b = \frac{1}{2} \rho U K L_e$ ;
- $L_e$ : is the length of fictitious element.

The “six-steps” iterative procedure, described in *Chap. 5.1*, was applied by using the same  $\Delta U$  adopted in the case of three unsteady actions. First torsional and vertical modes are analysed in the solution, in both symmetric and anti-symmetric configuration.

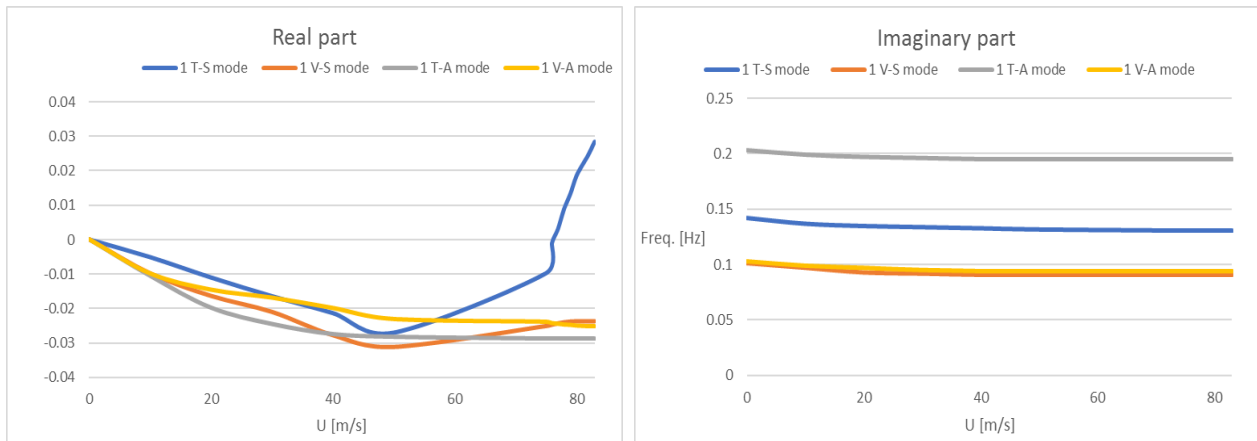


Figure 5-21: Real (left) and imaginary (right) part of the solution

. The analysis furnished a flutter critic speed  $U_f = 76.4$  m/s, associated to 1<sup>st</sup> T-S mode, (Figure 5-21) with an horizontal component of displacement, as in the three unsteady actions calculation, and a critical frequency of 0.131 Hz (Figure 5-20). As in the previous case, it is possible to observe that damped modal analysis gives a small reduction of vibration frequencies for each natural mode, as wind speed is increased.

The results are compared to those reported in the literature (“Bridge aeroelasticity”[6], “Aeroelastic phenomena”[15]), and with those obtained by Maldera in MATLAB (Table 5-6).

	<b>ANSYS results</b>	<b>Literature data</b>	<b>Analytic results</b>	<b>%err literature</b>	<b>%err analytic</b>
<b><math>U_{cr}</math> [m/s]</b>	76.4	77.7	75.6	1.7	1
<b><math>f_{cr}</math> [Hz]</b>	0.131	0.138	0.075	5.3	74

Table 5-6: Akashi Kaikyo Bridge flutter analysis, with two n-s actions and Drag steady, results comparison

The analysis, performed with Moment and Lift as unsteady actions plus steady Drag, gave very accurate results in terms of critical flutter speed: the relative error is always smaller than 2%. The horizontal effect, given by steady Drag, produces a destabilising effect that reduces the flutter critical wind speed of 4.9 m/s, respect to the three unsteady actions case. Another effect is the increasing of critical flutter frequency that reaches 0.131 Hz.

## ***Lift and Moment unsteady actions***

The last analysis developed considered only Lift and Moment, whereas Drag force on the bridge is not included at all. The flutter analysis was then performed considering Lift and Moment as unsteady actions.

The same “six-steps” procedure presented in *Chap. 5.1* was used. The fictitious element MATRIX27 is assembled as in the case of two unsteady actions. In fact, the terms in the matrices, which depending unsteady Drag, are imposed equal to zero and the final expressions of aeroelastic stiffness and damping is represented in *Eq. 5-14;5-15*.

The analysis was conducted up to a maximum wind speed of 100 m/s and first symmetric and anti-symmetric vertical and torsional modes were studied. The iterative procedure started from an initial wind speed of  $U_0 = 0$  m/s, and the increasing of wind speed  $\Delta U$  in the procedure was fixed to 10 m/s for each analysis up to  $U = 70$  m/s. After this point, the step-by-step discretization of  $\Delta U$  was set to  $\Delta U = 5$  m/s, until reaching the wind speed  $U_{max} = 100$  m/s.

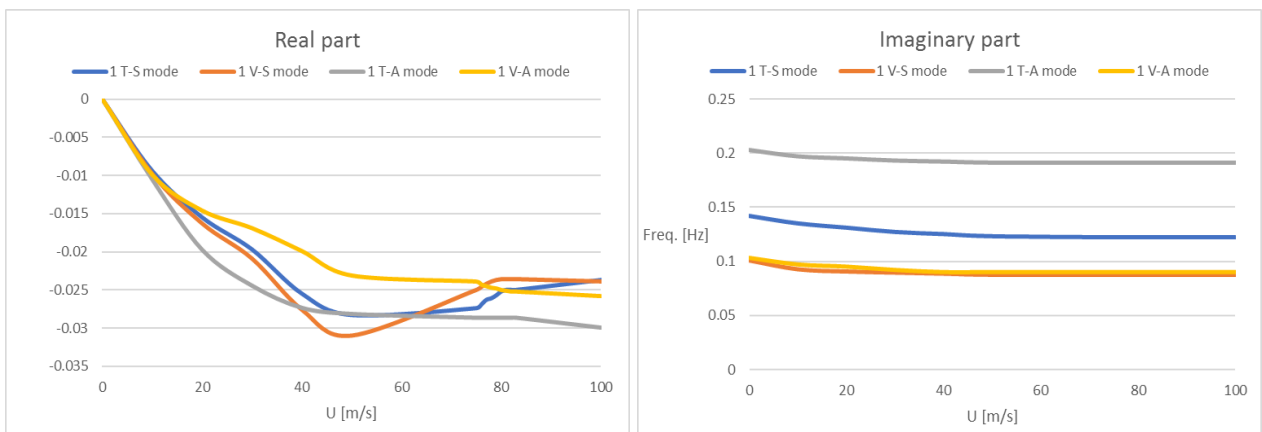


*Figure 5-22: Real (left) and imaginary (right) part of the solution*

No flutter was detected by this analysis in the 0-100 m/s wind speed range. In fact, the real part, that gives information about stability of the solution, assumes negative values along the wind speed interval considered for all modes analysed, included the first symmetric torsional mode, responsible of the instability in the two other cases. For this reason, it is possible to affirm that this last numerical model implemented in *ANSYS* was not able to obtain the correct solution for flutter instability.

# CHAPTER 6

## CONCLUSIONS

The finite element numerical modelling of long-span suspension bridges is a peculiar problem; in fact, such structures present a geometrically non-linear behaviour, because of the presence of hangers and main cables. The pre-loading of hangers and cables, produced by the bridge self-weight, causes an important stiffening effect that must be taken into account. So, it is necessary to use a software that is able to consider the said effect before solving an eigenvalue problem such that of a linearized stability analysis. Moreover, to perform a bridge flutter analysis, the software must also be able to model unsteady aerodynamic forces, such as the wind loads acting on oscillating bridge decks. By means of *ANSYS* software, it was possible to address both the previous issues. As concerns the modeling of cable and beam structures in *ANSYS*, the following finite elements were adopted:

- BEAM188 to model main cables and bridge deck;
- LINK180 to model hangers, that transmit only axial forces from the deck to main cables.

Some “test problems” were initially considered: a straight prestressed cable, a heavy parabolic cable, and 2D model of the Singapore Suspension Footbridge. The results, in terms of natural frequencies and modes, showed a very high accuracy compared to the analysis performed by other methods. In fact, *ANSYS* modal analyses displayed relative errors, in the evaluation of natural frequencies, smaller than 5% respect to analytic or numerical (*Lusas*) results. Another “validation problem” considered the case of an ideal suspension bridge, the one studied by Salvatori-Borri[5] *Chap. 3.1*.

As regards the original work of the thesis, a numerical study of the flutter problem of the *Akashi Kaikyo Bridge* was performed in *ANSYS*. Different models and analyses were realized. In all models, the unsteady wind actions, needed to perform flutter analysis, were modeled by using a specific element from the library: MATRIX27.

At first, a “Fish-bone” model was implemented and a flutter analysis was run by considering the unsteady forces of lift, drag, and moment. The analysis showed a good accuracy in predicting the critical flutter speed, but important differences were displayed with respect bibliographic data (“*Bridge aeroelasticity*”[6], “*Aeroelastic phenomena*”[15]), in terms of critical flutter frequency and respect the mode-shape responsible of the instability (*Table 6-1*). In fact, literature data indicate the first symmetric torsional mode associated to flutter phenomenon, whereas ANSYS “Fish-bone” numerical model identified the first symmetric vertical (bending) mode as responsible for flutter instability. In other words, the “Fish-bone” model was not able to describe the torsional behavior properly.

	<b>ANSYS results</b>	<b>Literature data</b>	<b>%err</b>
<b><math>U_{cr}</math> [m/s]</b>	77.2	77.7	0.6
<b><math>f_{cr}</math> [Hz]</b>	0.045	0.138	206

*Table 6-1: “Fish-bone” model flutter analysis results comparison*

The bridge model was improved by realising a “truss-beam” deck model that represents, with a better accuracy, the real structure of the *Akashi Kaikyo Bridge*. The aim of this model was to describe the torsional behaviour of the deck under wind more correctly and to obtain a better solution in terms of flutter wind speed, frequency and mode-shape. On this bridge model, three different flutter analyses were performed.

In the first analysis, three unsteady actions of lift, drag and moment were applied to the deck, obtaining, as it was expected, good results in terms of flutter wind speed, frequency, and mode shape (the first symmetric torsion mode).

In the second analysis, unsteady lift and moment actions, plus a steady drag force were applied to the deck: the results show an appreciable accuracy with respect to literature data, as in the previous case (*Table 6-2*). This is a very important result because it permits, in case of a numerical analysis performed in ANSYS, to evaluate the flutter critical speed and frequency correctly even if the flutter derivatives associated to drag forces ( $P_i$ ) are not available, provided the steady component of the drag force is considered (this requires knowing only the drag coefficient  $C_D$ ).

In the third calculation, flutter analysis was developed by including only the unsteady lift and moment forces, whereas the drag wind force was totally neglected. In this case, the analysis didn’t detect flutter instability for wind speeds up to 100 m/s, whereas for the two previous approaches the predicted critical wind speed was around 80 m/s. For this reason, it has been possible to assert that the horizontal wind load can’t be consider negligible when performing a flutter analysis on numerical models in ANSYS, at least for very long-span bridges like the *Akashi Kaikyo*.

	<b>ANSYS (<math>L_{ns}+D_{ns}+M_{ns}</math>)</b>	<b>ANSYS (<math>L_{ns}+M_{ns}+D_s</math>)</b>	<b>Analytic results</b>	<b>Literature data</b>	<b>% err <math>L_{ns}+D_{ns}+M_{ns}/</math> literature</b>	<b>% err <math>L_{ns}+M_{ns}+D_s/</math> literature</b>
<b><math>U_{cr}</math>[m/s]</b>	81.3	76.4	75.6	77.7	4.6	1.7
<b><math>f_{cr}</math>[Hz]</b>	0.122	0.131	0.075	0.138	13	5.3

*Table 6-2: "Truss-beam" model flutter critic speeds and frequencies comparison*

*Table 6-2* shows that the analysis with unsteady lift and moment ( $L_{ns}$ ,  $M_{ns}$ ) plus steady drag ( $D_s$ ), offered a higher accuracy than the analysis with three unsteady loads ( $L_{ns}$ ,  $M_{ns}$ ,  $D_{ns}$ ) with respect to the literature values, this both in terms of flutter speed and frequency. Considering the results, it can be noticed that the flutter critical frequency showed a relatively high sensitivity with respect to the model used to perform the analysis; conversely, the flutter critical speed showed a lower sensitivity.

Numerical models such the ones realised in this thesis can be used to develop wind analysis on suspension bridges to evaluate flutter instability. In fact, the showed procedure can be applied to other case studies to have a further validation of the numerical method, with the application to bridges presenting different lengths and deck structures.

## References

- [1] “suspension bridges Thangtong Gyalpo - Cerca con Google.” .
- [2] “The Innovation of Bridges timeline | Timetoast timelines.” [Online]. Available: <https://www.timetoast.com/timelines/the-innovation-of-bridges>.
- [3] “Problematiche aeroelastiche dei ponti di grande luce: stall flutter 1,” pp. 1–25.
- [4] Carpinteri Alberto, *Dinamica delle strutture*. 1998.
- [5] L. Salvatori and C. Borri, “Frequency- and time-domain methods for the numerical modeling of full-bridge aeroelasticity,” *Comput. Struct.*, vol. 85, no. 11–14, pp. 675–687, 2007.
- [6] F. N. & A. M. J.A. Jurado, S. Hernandez, *Bridge Aeroelasticity, sensitivity analysis and optimal design*. 2011.
- [7] D’argenio, “Instabilità aeroelastica dei ponti sospesi, un modello analitico con effetti del secondo ordine,” Politecnico di Torino, 2017.
- [8] B. Maldera, “Instabilità aeroelastica dei ponti sospesi: un modello analitico per lo studio del fenomeno del flutter,” Politecnico di Torino, 2017.
- [9] “4.188 BEAM188 3-D Linear Finite Strain Beam.” [Online]. Available: [http://www.ansys.stuba.sk/html/elem\\_55/chapter4/ES4-188.htm](http://www.ansys.stuba.sk/html/elem_55/chapter4/ES4-188.htm).
- [10] G. Forte, “Analisi geometricamente non lineare di ponti sospesi: la dinamica e l’instabilità flesso-torsionale del Tacoma Bridge,” Politecnico di Torino, 2017.
- [11] “LINK180.” [Online]. Available: [https://www.sharcnet.ca/Software/Ansys/17.0/en-us/help/ans\\_elem/Hlp\\_E\\_LINK180.html](https://www.sharcnet.ca/Software/Ansys/17.0/en-us/help/ans_elem/Hlp_E_LINK180.html).
- [12] Lacarbonara W., *Nonlinear structural mechanics: theory, dynamical phenomena, and modeling*, vol. 48, no. 10. 2013.
- [13] X. G. Hua, Z. Q. Chen, Y. Q. Ni, and J. M. Ko, “Flutter analysis of long-span bridges using ANSYS,” *Wind Struct.*, vol. 10, no. 1, pp. 61–82, 2007.
- [14] “4.27 MATRIX27 Stiffness, Damping, or Mass Matrix (UP19980821 ).” [Online]. Available: [http://www.ansys.stuba.sk/html/elem\\_55/chapter4/ES4-27.htm](http://www.ansys.stuba.sk/html/elem_55/chapter4/ES4-27.htm).
- [15] C. Borri and C. Mannini, *Aeroelstic phenomena and Pedestrian-Structure Dynamic Interaction on Non-Conventional Bridges and Footbridges*. 2010.